Molecular Structures and Energetics of the $(TiO_2)_n$ ($n = 1-4$) Clusters and Their Anions

Shenggang Li and David A. Dixon*

Chemistry Department, The University of Alabama, Shelby Hall, Box 870336, Tuscaloosa, Alabama 35487-0336

Received: January 8, 2008; Revised Manuscript Received: March 20, 2008

The $(TiO_2)_n$ clusters and their anions for $n = 1-4$ have been studied with coupled cluster theory [CCSD(T)] and density functional theory (DFT). For $n > 1$, numerous conformations are located for both the neutral and anionic clusters, and their relative energies are calculated at both the DFT and CCSD(T) levels. The CCSD(T) energies are extrapolated to the complete basis set limit for the monomer and dimer and calculated up to the triple-ζ level for the trimer and tetramer. The adiabatic and vertical electron detachment energies of the anionic clusters to the ground and first excited states of the neutral clusters are calculated at both levels and compared with the experimental results. The comparison allows for the definitive assignment of the ground-state structures of the anionic clusters. Anions of the dimer and tetramer are found to have very closely lying conformations within 2 kcal/mol at the CCSD(T) level, whereas that of the trimer does not. In addition, accurate clustering energies and heats of formation are calculated for the neutral clusters and compared with the available experimental data. Estimates of the titanium−oxygen bond energies show that they are stronger than the group VIB transition metal−oxygen bonds except for tungsten. The atomization energies of these clusters display much stronger basis set dependence than the clustering energies. This allows the calculation of more accurate heats of formation for larger clusters on the basis of calculated clustering energies.

1. Introduction

Titanium dioxide (TiO_2) is the technologically most important compound formed by group IVB transition metal elements and is widely used as a white pigment.[1,2] It has been applied both as a catalyst support[3] and as a photocatalyst.[4,5] The photocatalytic activity of titanium dioxide has been widely studied for solar energy conversion,[6] as well for removal of organic pollutants from aqueous waste streams.[7]

At room temperature, bulk TiO_2 exists in three natural phases: rutile, anatase, and brookite.[1] The rutile phase is the most common phase, and at elevated temperature the other phases transform into rutile. In all three phases, the Ti atom is surrounded by six O atoms in distorted octahedral configurations, and the O atom is surrounded by three Ti atoms in trigonal planar configurations (see the Supporting Information for structures of the rutile and anatase phases).[8–13] In both the rutile and anatase phases, all of the titanium and oxygen centers are equivalent, whereas they are not in the brookite phase due to the higher order of distortion.[8,13] In the rutile phase, the TiO_6 octahedron is stretched along the axial direction resulting in two longer Ti−O bonds (1.982 Å) and four shorter ones (1.947 Å).[8] In addition, the O−Ti−O bond angles in the equatorial plane are distorted from 90° to 81.1° and 98.9°, and the Ti−O bonds in the equatorial plane remain perpendicular to those along the axial direction.[8] In the anatase phase, in addition to the distortion along the axial direction, which results in two longer Ti−O bonds (1.980 Å) and four shorter ones (1.934 Å), the Ti−O bonds in the equatorial plane are no longer perpendicular to those in the axial direction.[13] These Ti−O bonds in the equatorial plane are distorted so that the O−Ti−O bond angles between the adjacent Ti−O bonds all equal 92.4°.[13] Furthermore, the anatase phase is found to be photocatalytically active. Although the rutile phase is more stable than the anatase phase at room temperature and ambient pressure, experimental and theoretical studies have suggested the anatase phase to be more stable than the rutile phase when the particle size is smaller than ∼14 nm.[14,15] More recently, the anatase phase has been calculated to be more stable than the rutile phase at 0 K and ambient pressure.[16]

Due to its technological importance, numerous experimental and theoretical studies have been carried out on isolated titanium oxide clusters to correlate their structures and properties with those of the bulk. An early electric dipole moment measurement by electric quadrupole field deflection of molecular beams of MO_2 (M = Si, Ti, Zr, Ce, Th, Ta, U) showed that all of these dioxides are polar except for SiO_2.[17] Matrix infrared (IR) spectroscopy has been used to study TiO and TiO_2,[18] and the reaction products of Ti, Zr, and Hf atoms with molecular oxygen.[19] The O═Ti═O bond angle in TiO_2 was estimated to be 110 ± 15° from Ti isotope splittings[18] and was further refined to 113 ± 5° in a subsequent experiment with reduced spectral line widths.[19] The bond angle in TiO_2^- has also been estimated to be 128 ± 5°.[19] In addition, an emission system has been observed at ∼530 nm for TiO_2.[18] High temperature mass spectroscopic measurements of the vapors over the europium−titanium−oxygen and cobalt−titanium−oxygen systems yielded estimated total atomization energies for TiO_2 and Ti_2O_4 of 301 ± 3 and 721 ± 11 kcal/mol at 0 K.[20,21] Mass spectrometry has been employed to study the reaction products of 29 transition metal cations with molecular oxygen,[22] the formation and fragmentation of titanium oxide cluster cations,[23] and the reaction products of small titanium oxide cluster cations toward molecule oxygen.[24] Early transition metal cations were shown to form oxide cations by oxygen atom abstraction, whereas late transition metal cations by molecular oxygen addition.[22] Titanium oxide cluster cations of the form $Ti_nO_{2n-m}^+$ were observed for $n = 1-8$ and $m = 0-4$ by sputtering titanium foil exposed to oxygen, and for $n = 1-7$ and $m = 1-3$ by sputtering titanium

* Corresponding author. E-mail: dadixon@bama.ua.edu.

10.1021/jp800170q CCC: $40.75
Published on Web 06/26/2008

dioxide powder.[23] A simple pair potential ionic model has been used to calculate the structures of the Ti_nO_{2n-m} clusters for $m = 0-2$, and no distinct structures were found for $m = 1$ and $m = 2$, whereas the Ti_nO_{2n} clusters were found to have pendant and terminal oxygen atoms.[23] Furthermore, the $Ti_nO_{2n+m}^+$ clusters with $n \geq 3$ for $m = 0$ and $n \geq 2$ for $m = 1$ were found to be inert toward the reaction of molecule oxygen.[24] Anion photoelectron spectroscopy (PES) has been used to study TiO_m^- and $Ti_nO_{2n}^-$ clusters for $m = 1-3$ and $n = 2-10$ at wavelengths up to 157 nm.[25,26] Electron detachment energies have been measured for these clusters, and the energy difference between the ground state of the neutral and its first excited state (band gap) has been shown to be strongly size-dependent for $n \leq 6$, and to rapidly approach the bulk limit for $n \geq 7$.[26] Most of the PES features are very broad, indicative of large geometry changes upon photodetachment, and this feature has been attributed to the localization of the extra electron in the anions.[26] Single-photon and multiphoton ionization experiments have been carried out on the titanium oxide clusters formed by reactions of metal atoms with molecule oxygen.[27,28] The Ti_nO_{2n} and Ti_nO_{2n+1} clusters were found to be the most stable neutral clusters, and the Ti_nO_{2n-1} and Ti_nO_{2n-2} clusters were formed by fragmentation.[28] Infrared resonance enhanced multiphoton ionization (IR-REMPI) spectroscopy has been applied to study titanium oxide clusters in the gas phase, and their structures were shown to be close to that for the rutile phase of bulk TiO_2.[29,30]

Theoretical studies on the titanium oxide clusters have mostly been carried out at the density functional theory (DFT)[31] level, although a number of wave function-based methods have also been employed. For the monomer, an early configuration interaction calculation with single and double excitations (CISD) and Davidson correction for the quadruple excitations was performed for the ground state ($^1A_1$) and the lowest energy B_2 excited state, and good agreement with experiment was found for the geometry, but not for the symmetric stretching frequency.[32] In addition, the $^1B_2$ and $^3B_2$ excited states were found to be nearly degenerate with a linear geometry.[32] Bergstrom et al. benchmarked the performance of a number of exchange−correlation functionals for the calculation of the geometries, ionization energies, dipole moments, atomization energies, and harmonic frequencies for TiO, TiO_2, and Ti_2 against the Hartree−Fock (HF), second order Møller−Plesset perturbation theory (MP2), and CISD methods.[33] Most of the DFT functionals benchmarked including BLYP,[34,35] BP86,[34,36] B3LYP,[37,35] and B3P86[37,36] were found to provide superior results to the three wave function-based methods, and exchange−correlation functionals without HF exchange (pure functionals) were found to outperform those with HF exchange (hybrid functionals).[33] The DFT results are consistent with our recent benchmarking studies of group VIB metal-oxide clusters.[38] Walsh et al. calculated the ground-state geometries and energetics for TiO_m ($m = 1-3$) and their anions at the DFT level and at the coupled cluster level with single and double excitations and a perturbative triples correction [CCSD(T)][39–42] level.[43] The ground state of TiO_2^- was predicted to be the $^2A_1$ state of C_{2v} symmetry, and the adiabatic electron detachment energy (ADE) calculated at the CCSD(T) level was found to be in good agreement with experiment.[43] DFT calculations on the first row transition metal dioxides and their anions predicted that their ground states have the oxo form (O═M═O) except for copper dioxide, which has a superoxo form (M−O−O).[44] Their calculated electron affinity for TiO_2 is slightly lower than the experimental value.[44] Very recently, multireference (MR) CISD calculations with Davidson corrections have been carried out for the low-lying states of TiO_2, and the geometries and energies at the MR-CISD level were found to be similar to those at the DFT level.[45]

HF calculations have been performed on the larger clusters, Ti_nO_{2n} and Ti_nO_{2n-1}, for $n = 1-3$.[46] A C_{2h} structure with two bridge and two terminal oxygen atoms was calculated to be the ground state of Ti_2O_4, and a C_s structure with a linear configuration of the titanium atoms was calculated to be the ground state of Ti_3O_6.[46] DFT in the local spin density approximation (LSDA) with plane-wave basis sets has been used to calculate the Ti_nO_{2n} and Ti_nO_{2n+1} clusters for $n = 1-3$ and their anions and cations.[47] The same C_{2h} structure for Ti_2O_4 was predicted to be the ground state, but for Ti_3O_6, a C_s structure with a triangular configuration of the titanium atoms was calculated to be its ground state.[47] For $Ti_2O_4^-$, a C_{3v} structure with three bridge oxygen atoms were found to be more stable than the C_{2h} structure by 0.02 eV, and the calculated ADEs for the C_{3v} and C_{2h} structures are lower than the experimental value by ∼0.8 and ∼0.4 eV, respectively.[47] For $Ti_3O_6^-$, the ADE of the C_s structure with a triangular configuration of the titanium atoms was lower than the experimental value by ∼0.5 eV.[47] The structures of the Ti_nO_mclusters for $n = 1-6$ and $m = 1-12$ have been calculated at the B3P86/6-31G(d) level.[48] For Ti_2O_4, only the C_{2h} structure was located; for Ti_3O_6, the structure with a linear configuration for the titanium atoms was calculated to have C_2 symmetry; and for Ti_4O_8, a C_{2h} structure with a linear configuration for all the titanium atoms was obtained.[48] Employing a combination of simulated annealing, Monte Carlo basin hopping (SA-MCBH) simulations, and genetic algorithm (GA) techniques, low energy structures for the Ti_nO_{2n} clusters for $n = 1-15$ were generated and subsequently refined by DFT calculations.[49] The structure for Ti_2O_4 is similar to the C_{2h} structure, although it appears to have D_{2h} symmetry; for Ti_3O_6, the C_s structure with a triangular configuration for the titanium atoms was predicted to be the most stable structure; and for Ti_4O_8, a structure with C_{2v} symmetry was predicted to be the most stable.[49] The structures for Ti_nO_{2n} clusters for $n = 1-9$ and their anions and cations have also been calculated by Qu and Kroes at the B3LYP/LANL2DZ level.[50] For Ti_2O_4, the C_{2h} structure was again predicted to be the most stable; for Ti_3O_6, the C_s structure with a triangular configuration for the titanium atoms was predicted to be the most stable; and for Ti_4O_8, another structure with C_{2v} symmetry different from that found by Hamad et al.[47] was predicted to be the most stable.[50] For $Ti_2O_4^-$, the C_{2h} structure was predicted to be the most stable, and its ADE was calculated to be very close to the experimental value; for $Ti_3O_6^-$, the C_s structure with a triangular configuration for the titanium atoms was predicted to be the most stable, but its ADE was calculated to be ∼0.5 eV higher than the experimental value; and for $Ti_4O_8^-$, the same C_{2v} structure was predicted to be the most stable, but its ADE was predicted to be higher than the experimental value by ∼0.4 eV.[50]

The above survey of previous studies on small titanium oxide clusters clearly shows that the structures of these clusters are still not well-established, and there are still fairly large discrepancies between the experimental and theoretical electron detachment energies. For example, the ADEs of $Ti_2O_4^-$ and $Ti_3O_6^-$ calculated by Albaret et al. at the LSDA level with plane-wave basis sets are lower than the experimental values by ∼0.4 and 0.5 eV, respectively.[47] Although the ADE of $Ti_2O_4^-$ calculated by Qu and Kroes at the B3LYP/LANL2DZ level is in good agreement with the experimental value, their calculated ADEs for $Ti_3O_6^-$ and $Ti_4O_8^-$ are higher than the experimental values by ∼0.5 and ∼0.4 eV respectively.[50]

In our recent benchmark studies on the electron detachment energies of the group VIB transition metal oxide clusters,[38] we showed that (1) the CCSD(T) method with a sufficiently large basis set and the inclusion of core−valence correlation corrections can reproduce the experimental detachment energies to better than 0.1 eV if the electronic wave function is dominated by a single determinant; (2) the BP86 and PW91 functionals provide the best overall electron detachment energies for these oxide clusters; and (3) the B3LYP functional does not perform well for the first row transition metal. Thus the discrepancies between the experimental and theoretical electron detachment energies can arise either from incorrectly predicted ground-state structures or from the systematic error of the functional in the predicted electron detachment energies.

In the current study, we use both density functional theory (DFT) and coupled cluster theory [CCSD(T)] to calculate the structural and energetic properties of the $(TiO_2)_n$ ($n = 1-4$) clusters and their anions. Relative energies of the different conformations, and comparison of the calculated ADEs and VDEs for the different conformations of the anionic clusters with the experimental results allow us to firmly establish the ground-state structures of these clusters. In addition, the clustering energies and heats of formation of the neutral clusters are calculated to provide accurate thermodynamic data for these transition metal oxide clusters.

2. Computational Methods

Equilibrium geometries and harmonic vibrational frequencies were calculated at the DFT level with the B3LYP exchange−correlation functionals for both the neutral and anionic clusters. No scaling factors were applied to any of the calculated frequencies. Due to the potential for artificial symmetry breaking as discussed below with the B3LYP functional for several anionic clusters in this study, we used the ZPEs calculated at the BP86/aD level. For the low-lying structures, geometries and frequencies were also calculated with the BP86 and PW91[51,52] functionals. We used the augmented correlation-consistent aug-cc-pV*n*Z basis set for O,[53] and the aug-cc-pV*n*Z-PP effective core potential (ECP) basis sets[54] for Ti in the DFT optimization and frequency calculations with n = D and additional DFT single point energy calculations with n = T; these basis sets are collectively denoted as aD and aT. The DFT energies given in the tables below were obtained with the aT basis set. The DFT energies with the aD basis set are given as Supporting Information. These results show that the various DFT energies do not exhibit a strong dependence on the basis set with most energies differing by up to ~1 kcal/mol.

For the monomer and dimer, we optimized the geometries of the low-lying structures at the CCSD(T) level[39–42] with the aD and aT basis sets. For the monomer, the harmonic frequencies were calculated at the CCSD(T)/aT level. For the monomer and dimer, the CCSD(T) energy calculations were also performed with the aQ basis set. The CCSD(T) energies were extrapolated to the complete basis set (CBS) limit using a mixed Gaussian/exponential formula.[55] The cardinal numbers for the aD, aT, and aQ basis sets we used are 2, 3, and 4. Our recent studies on the group VIB transition metal oxide clusters have shown that the effect of the choice of the cardinal numbers in this extrapolation scheme is fairly small.[38] Core−valence correlation corrections were calculated at the CCSD(T) level with the aug-cc-pwCV*n*Z basis set for O,[56,57] and the aug-cc-pwCV*n*Z-PP basis set for Ti,[54] with n = D and T. These basis sets will be collectively denoted as awCVDZ and awCVTZ, respectively. In addition, relativistic corrections were calculated as expectation values of the mass−velocity and Darwin terms (MVD) of the CISD wave function with the aT basis set. A potential problem arises in computing the scalar relativistic correction for the molecules in this study as there is the possibility of "double counting" the relativistic effect on the metal when applying a MVD correction to an energy that already includes some relativistic effects via the relativistic ECP. Because the MVD operators mainly sample the core region where the pseudo-orbitals are small, we assume any double counting to be small. The above approach follows on ours and others' work on the accurate prediction of the heats of formation for a wide range of compounds.[58–72]

For the trimer and tetramer, the CCSD(T) calculations were performed with the aD and aT basis sets at the B3LYP/aD geometries. Core−valence correlation corrections were calculated at the CCSD(T) level with awCVDZ basis sets, and scalar relativistic corrections were calculated as expectation values of the MVD terms for the CISD/aT wave function.

Time-dependent DFT (TD-DFT)[73–79] at the B3LYP/aD, BP86/aD, and PW91/aD levels is employed to calculate the vertical excitation energies of the ten lowest singlet and triplet excited states at the optimized geometries of the low-lying neutral structures. An asymptotic correction[78,79] for the exchange−correlation functional was employed for the B3LYP functional; this has very small effects on the transition energies of the low-lying excited states.[80]

The DFT geometry optimization and frequency calculations were performed with the Gaussian 03 program package.[81] For the pure DFT methods, the density fitting approximation was employed to speed up the calculations.[82,83] The density fitting sets were automatically generated from the atomic orbital primitives. The TD-DFT calculations were performed with the NWChem 5.0 program packages.[84,85] The CCSD(T) calculations were performed with the MOLPRO 2006.1 program package.[86] The open-shell calculations were done with the R/UCCSD(T) approach where a restricted open shell Hartree−Fock (ROHF) calculation was initially performed and the spin constraint was then relaxed in the coupled cluster calculation.[87–89] The calculations were performed on the Opteron-based Cray XD1 and Itanium 2-based SGI Altix supercomputers at the Alabama Supercomputer Center, the Xeon-based Dell Linux cluster at the University of Alabama, the local Opteron-based Parallel Quantum Solutions Linux cluster, and the Itanium 2-based Linux cluster at the Molecular Science Computing Facility from the Pacific Northwest National Laboratory.

Multidimensional Franck−Condon factors (FCFs) for the vibronic transitions from the ground state of the anion to that of the neutral cluster were calculated within the harmonic approximation to simulate the photoelectron spectrum. These FCFs were calculated[90] using the recursion relations derived by Doktorov et al.[91] adapted from the work of Yang et al.[92] The three-level binary tree algorithms of Ruhoff and Ratner,[93] originated from the binary tree algorithm of Gruner and Brumer,[94] have been implemented. In addition, the backtracking algorithm by Kemper et al.[95] has been implemented to generate all of the vibrational states to be calculated at a given level. The backtracking algorithm also allows for the efficient utilization of the calculated integrals. In simulating the spectra, the theoretical equilibrium geometries, harmonic frequencies, and normal coordinates were used. Our program interfaces with Gaussian 03, MOLPRO, and NWChem. A Boltzmann distribution was used to account for the finite temperature effect with a Lorentzian line shape with an experimental line width.

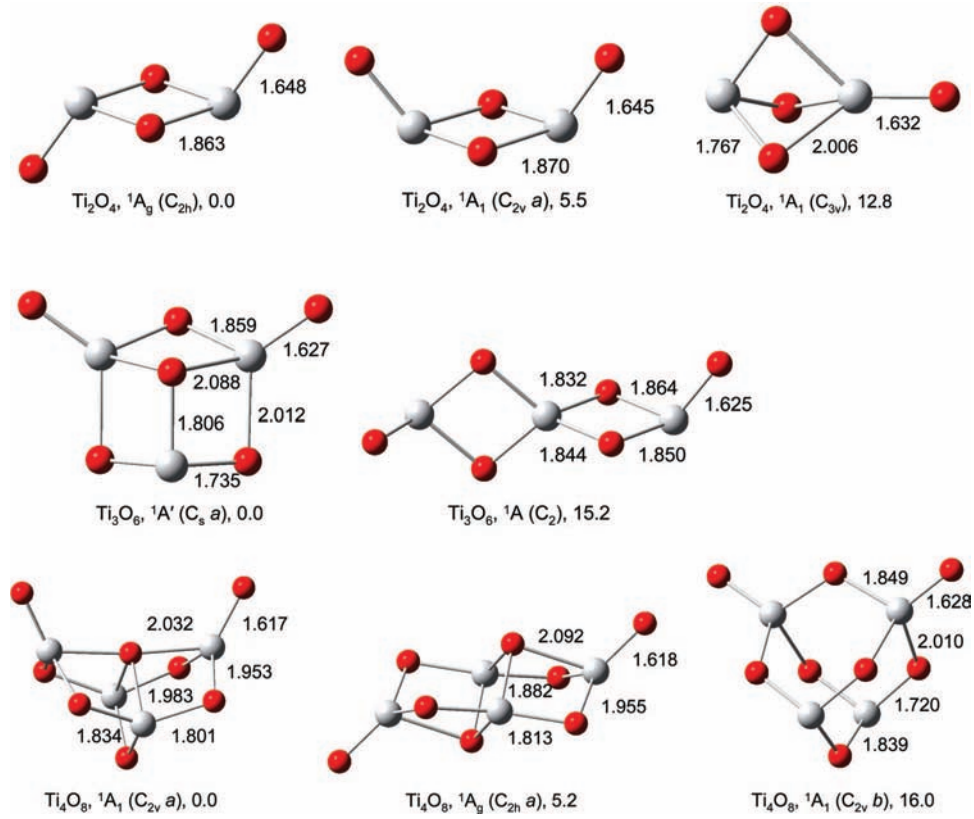

Figure 1. Low-lying structures of $(TiO_2)_n$ ($n = 2-4$). The bond lengths (Å) shown are calculated at the CCSD(T)/aT level for $n = 2$ and at the B3LYP/aD level for $n = 3$ and 4. The relative energies (kcal/mol) shown are calculated at the CCSD(T)/CBS level for $n = 2$ and at the CCSD(T)/aT//B3LYP/aD level for $n = 3$ and 4.

Following our previous work on the group VIB transition metal oxide clusters,[96] the normalized and differential clustering energies, $\Delta E_{\mathrm{norm},n}$ and $\Delta E_{\mathrm{diff},n}$, are defined by

$$\Delta E_{\mathrm{norm},n} = [nE(TiO_2) - E(Ti_nO_{2n})]/n \quad (1)$$

$$\Delta E_{\mathrm{diff},n} = [E(Ti_{n-1}O_{2n-2}) + E(TiO_2) - E(Ti_nO_{2n})] \quad (2)$$

The normalized clustering energy is the average binding energy of the monomer in a cluster, and the differential clustering energy is the energy required to remove one monomer from the cluster.

Atomization energies of the $(TiO_2)_n$ ($n = 1-4$) clusters at 0 K were calculated as the energy differences between the ground states of the atoms and those of the clusters following our previous work:[38]

$$D_{0,0K} = \Delta E_{CBS} + \Delta E_{ZPE} + \Delta E_{CV} + \Delta E_{SR} + \Delta E_{SO} \quad (3)$$

where each individual term was evaluated as in

$$\Delta E = nE(Ti,{}^3F) + 2nE(O,{}^3P) - E(Ti_nO_{2n}) \quad (4)$$

The spin−orbit contribution for the ground state of O (^3P) is −0.223 kcal/mol and that of Ti (^3F) is −0.636 kcal/mol.[97] For the B3LYP, BP86, and PW91 methods, eq 3 reduces to

$$D_{0,0K} = \Delta E_e + \Delta E_{ZPE} + \Delta E_{SO} \quad (5)$$

Heats of formation of the clusters at 0 K are calculated from the atomization energies and the experimental heats of formation for the atoms as given in

$$\Delta H_{f,0K}(Ti_nO_{2n}) = n\Delta H_{f,0K}(Ti) + 2n\Delta H_{f,0K}(O) - D_{0,0K}(Ti_nO_{2n}) \quad (6)$$

The heats of formation at 0 K for the elements in the gas phase are $\Delta H_f^0(O) = 58.98 \pm 0.02$ kcal/mol,[98] and $\Delta H_f^0(Ti) = 112.4 \pm 0.7$ kcal/mol.[99] The JANAF heat of formation of Ti(g) at 0 K is $\Delta H_f^0(Ti) = 112.55 \pm 4.0$ kcal/mol with a much larger error bar.[98] Heats of formation at 298 K are calculated by following the procedures outlined by Curtiss et al.[100]

3. Results and Discussion

3.1. Equilibrium Geometries of Neutral Clusters. Optimized molecular structures for the low-lying states of the $(TiO_2)_n$ ($n = 2-4$) clusters are shown in Figure 1, and those for their anions are shown in Figure 2. Additional conformations (we use the term conformer for these structures to include the term isomer) with higher energies are shown in Figure 3 for the neutral and those for the anionic clusters are given as Supporting Information. Also given in these figures are the optimized titanium−oxygen bond lengths and calculated relative energies. The titanium−oxygen bond lengths and bond angles calculated at all the levels are given as Supporting Information for the monomer and dimer. The calculated relative energies for these low-lying states are shown in Tables 1 and 2 at the CCSD(T) and DFT levels. The CCSD(T) relative energies include a number of different contributions to show their relative importance: the basis set extrapolation to the complete basis set (CBS) limit where possible, the zero-point energy (ZPE) correction, the core−valence (CV) correction, and the scalar relativistic (SR) correction. This information is critical to provide insight into the potential sources of error when applying the CCSD(T) method for larger clusters.

3.1.1. Monomer. The ground state of TiO_2 is predicted to be $^1A_1$ in C_{2v} symmetry. The calculated O═Ti═O bond angle of 112.4° at the CCSD(T)/aT level is in excellent agreement with the experimental result of 113 ± 5°.[19] The CCSD(T)/aT value for the Ti═O bond length is 1.666 Å.

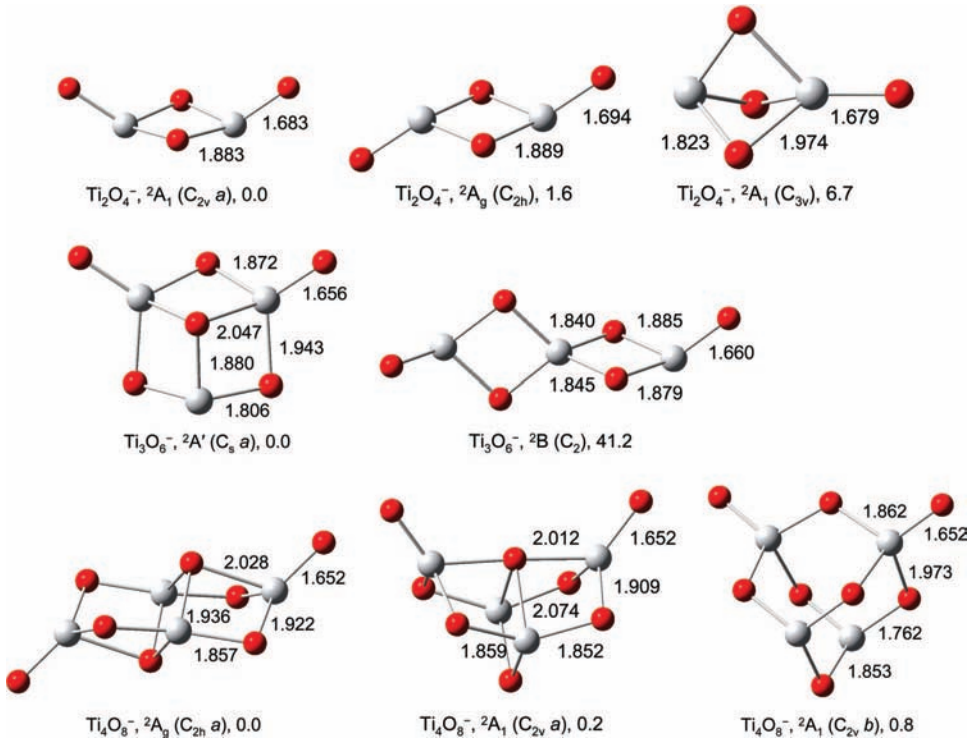

Figure 2. Low-lying structures of $(TiO_2)_n^-$ ($n = 2-4$). The bond lengths (Å) shown are calculated at the CCSD(T)/aT level for $n = 2$ and at the B3LYP/aD level for $n = 3$ and 4. The relative energies (kcal/mol) shown are calculated at the CCSD(T)/CBS level for $n = 2$ and at the CCSD(T)/aT//B3LYP/aD level for $n = 3$ and 4.

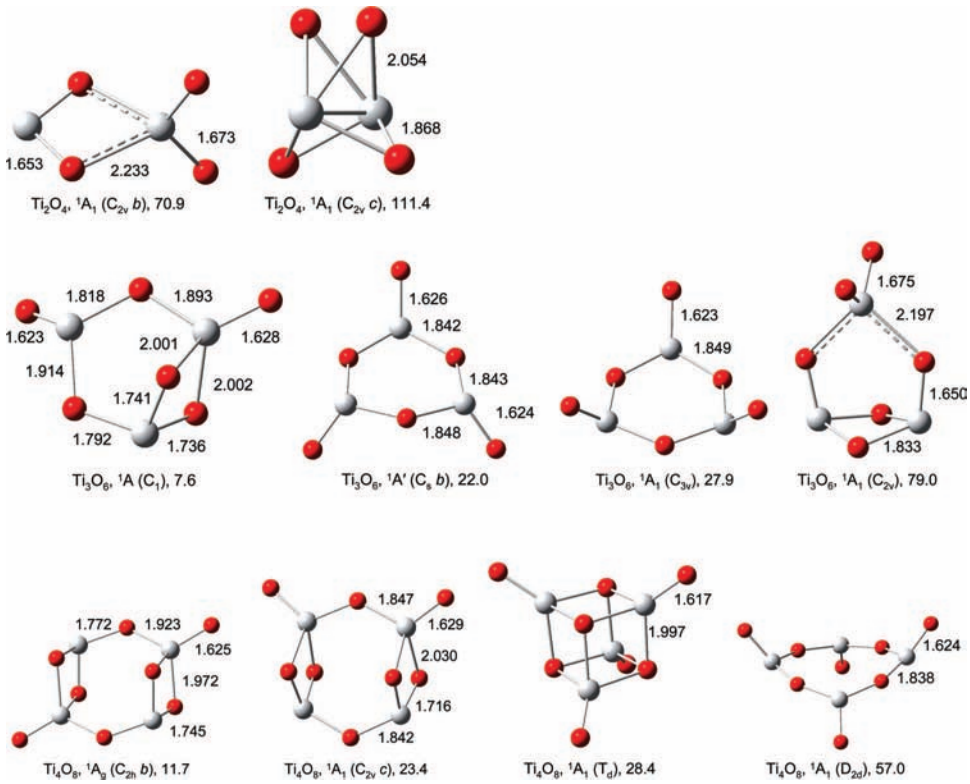

Figure 3. Additional structures of $(TiO_2)_n$ ($n = 2-4$). The bond lengths (Å) and relative energies (kcal/mol) shown are calculated at the B3LYP/aD level.

3.1.2. Dimer. The ground state of Ti_2O_4 is predicted to be ^1A_g in C_{2h} symmetry. As shown in Figure 1, there are two low-lying conformers besides the C_{2h} structure. At the CCSD(T)/CBS level, the $^1A_1$ state of the (C_{2v} **a**) structure is predicted to be 5.5 kcal/mol higher in energy than the C_{2h} structure, and the $^1A_1$ state of the C_{3v} structure is predicted to be 12.8 kcal/mol higher in energy than the C_{2h} structure. The C_{2h} and (C_{2v} **a**) structures are very similar, both of which have two bridge and two terminal oxygen atoms. The difference is that the C_{2h} structure has a *trans* configuration for the two terminal oxygen atoms, whereas the (C_{2v} **a**) structure has a *cis* configuration. In contrast, the C_{3v} structure has three bridge and one terminal

TABLE 1: Relative Energies at 0 K (ΔE_{0K}, kcal/mol) for the Low-Lying States of $(TiO_2)_n$ and $(TiO_2)_n^-$ ($n = 2-4$) Calculated at the CCSD(T) Level

molecule	state	ΔE_{aD}[a]	ΔE_{aT}[b]	ΔE_{aQ}[b]	ΔE_{CBS}[c]	$\Delta E_{CV(D)}$[b,d]	$\Delta E_{CV(T)}$[b,e]	ΔE_{SR}[b,f]	ΔE_{ZPE}[g]	ΔE_{0K}[h]
Ti_2O_4	^1A_g (C_{2h})	0.00	0.00	0.00	0.00	0.00	0.00	0.00	0.00	0.0
	$^1A_1$ (C_{2v} **a**)	5.37	5.48	5.44	5.40	+0.15	+0.24	−0.01	−0.09	5.5
	$^1A_1$ (C_{3v})	15.37	14.31	14.23	14.20	−1.95	−1.02	+0.09	−0.43	12.8
Ti_3O_6	$^1A'$ (C_s **a**)	0.00	0.00			0.00		0.00	0.00	0.0
	^1A (C_2)	15.39	14.76			+0.39		+0.02	−0.01	15.2
Ti_4O_8	$^1A_1$ (C_{2v} **a**)	0.00	0.00			0.00		0.00	0.00	0.0
	^1A_g (C_{2h} **a**)	4.78	6.06			−0.68		+0.02	−0.19	5.2
	$^1A_1$ (C_{2v} **b**)	13.68	13.26			+3.35		−0.15	−0.49	16.0
$Ti_2O_4^-$	$^2A_1$ (C_{2v} **a**)	0.00	0.00	0.00	0.00	0.00	0.00	0.00	0.00	0.0
	^2A_g (C_{2h})	1.46	1.61	1.55	1.50	+0.18	+0.21	−0.02	−0.06	1.6
	$^2A_1$ (C_{3v})	9.30	8.18	8.02	7.96	−1.93	−1.42	−0.04	+0.16	6.7
$Ti_3O_6^-$	$^2A'$ (C_s **a**)	0.00	0.00			0.00		0.00	0.00	0.0
	^2B (C_2)	41.08	40.67			+1.03		+0.19	−0.67	41.2
$Ti_4O_8^-$	^2A_g (C_{2h} **a**)	0.00	0.00			0.00			0.00	0.0
	$^2A_1$ (C_{2v} **a**)	0.98	−0.21			+0.41			−0.03	0.2
	$^2A_1$ (C_{2v} **b**)	−0.55	−1.63			+2.43			−0.01	0.8

[a] Geometries from CCSD(T)/aD for $n = 2$, and from B3LYP/aD for $n = 3$ and 4. [b] Geometries from CCSD(T)/aT for $n = 2$, and from B3LYP/aD for $n = 3$ and 4. [c] Extrapolated using the mixed Gaussian/exponential formula for the CCSD(T) energies with the aD, aT, and aQ basis sets. [d] CCSD(T)/awCVDZ. [e] CCSD(T)/awCVTZ. [f] CISD/aT. [g] BP86/aD. [h] $\Delta E_{0K} = \Delta E_{CBS} + \Delta E_{CV(T)} + \Delta E_{SR} + \Delta E_{ZPE}$ for $n = 2$, and $\Delta E_{aT} + \Delta E_{CV(D)} + \Delta E_{SR} + \Delta E_{ZPE}$ for $n = 3$ and 4.

TABLE 2: Relative Energies at 0 K (ΔE_{0K}, kcal/mol) for the Low-Lying States of $(TiO_2)_n$ and $(TiO_2)_n^-$ ($n = 2-4$) Calculated at the CCSD(T), B3LYP/aT//B3LYP/aD, BP86/aT//BP86/aD, and PW91/aT//PW91/aD Levels

		CCSD(T)[a,b]	B3LYP[a]	BP86	PW91
		$(TiO_2)_n$			
Ti_2O_4	^1A_g (C_{2h})	0.0	0.0	0.0	0.0
	$^1A_1$ (C_{2v} **a**)	5.5	5.7	6.1	6.2
	$^1A_1$ (C_{3v})	12.8	14.9	13.3	12.5
Ti_3O_6	$^1A'$ (C_s **a**)	0.0	0.0	0.0	0.0
	^1A (C_2)	15.2	8.8	7.5	8.3
Ti_4O_8	$^1A_1$ (C_{2v} **a**)	0.0	0.0	0.0	0.0
	^1A_g (C_{2h} **a**)	5.2	6.0	4.8	4.9
	$^1A_1$ (C_{2v} **b**)	16.0	8.5	9.6	10.1
		$(TiO_2)_n^-$			
$Ti_2O_4^-$	$^2A_1$ (C_{2v} **a**)	0.0	0.0	0.0	0.0
	^2A_g (C_{2h})	1.6	0.1	−0.3	−0.4
	$^2A_1$ (C_{3v})	6.7	7.5	7.8	6.8
$Ti_3O_6^-$	$^2A'$ (C_s **a**)	0.0	0.0	0.0	0.0
	^2B (C_2)	41.2	30.7	22.6	23.4
$Ti_4O_8^-$	^2A_g (C_{2h} **a**)	0.0	0.0	0.0	0.0
	$^2A_1$ (C_{2v} **a**)	0.2	−0.3	0.3	0.1
	$^2A_1$ (C_{2v} **b**)	0.8	−5.6	−4.7	−4.6

[a] ZPEs from BP86/aD. [b] CCSD(T)/CBS for $n = 2$, and CCSD(T)/aT for $n = 3$ and 4.

oxygen atoms. The calculated Ti═O bond lengths at the CCSD(T)/aT level for the C_{2h} and C_{2v} structures are ~0.02 Å shorter than that in the monomer, and that in the C_{3v} structure is ~0.03 Å shorter. The calculated Ti−O bond lengths at the CCSD(T)/aT level for the C_{2h} and C_{2v} structures are ~0.20 Å longer than the Ti═O bond length in the monomer, whereas for the C_{3v} structure, three of the Ti−O bonds are ~0.10 Å longer, and the other three are ~0.34 Å longer. Thus, the C_{3v} structure can be considered as a Ti(−O)$_3$ unit interacting with a Ti═O unit. In addition, two more conformers of C_{2v} symmetry (Figure 3) lie much higher in energy than the C_{2h} structure, by 70.9 and 111.4 kcal/mol, respectively, at the B3LYP/aD level. The (C_{2v} **b**) structure is best described as two weakly interacting monomers, and the (C_{2v} **c**) structure is best described as Ti_2O_2 weakly interacting with O_2. The C_{2h} structure has been predicted to be the ground state of Ti_2O_4 in most previous studies, although the structures calculated using a pair-potential ionic model,[23] and using the SA-MCBH and B3LYP/DZVP approaches[49] appear to have D_{2h} symmetry.

3.1.3. Trimer. The ground state of Ti_3O_6 is predicted to be $^1A'$ in C_s symmetry. It has a six-member ring formed from three −(Ti−O)− units, a triple-bridge oxygen atom at the center, and two terminal oxygen atoms. Its stability may be due to its closely packed structure. A number of low-lying structures were located for the trimer. A C_1 structure (Figure 3) formed by moving the triple-bridge oxygen atom in the (C_s **a**) structure away from one of the titanium atoms with a terminal oxygen atom lies higher than the (C_s **a**) structure by 7.6 kcal/mol at the B3LYP/aD level and by 9.7 kcal/mol at the CCSD(T)/aD//B3LYP/aD level. However, geometry optimizations at the BP86/aD and PW91/aD levels starting from this C_1 structure led to the (C_s **a**) structure, suggesting that the C_1 structure may not be a true local minimum. A C_2 structure formed by linearly extending the ground-state structure of Ti_2O_4 with another TiO_2 unit is calculated to be higher in energy than the (C_s **a**) structure by 15.2 kcal/mol at the CCSD(T)/aT//B3LYP/aD level. The other structures for the trimer (Figure 3) lie even higher in energy. The (C_s **b**) and C_{3v} structures with a six-member ring and three terminal oxygen atoms lie higher in energy than the (C_s **a**) structure by 22.0 and 27.9 kcal/mol at the B3LYP/aD level and by 29.1 and 34.4 kcal/mol at the CCSD(T)/aT//B3LYP/aD level. These two structures are similar to the ground-state structures of M_3O_9 (M = Cr, Mo, W)[96] except that they have one less terminal oxygen atom on each metal center. The C_{2v} structure with a dimer weakly interacting with a monomer lies 79.0 kcal/mol higher in energy than the (C_s **a**) structure at the B3LYP/aD level. The (C_s **a**) structure has been predicted to be the ground state of Ti_3O_6 at the LSDA level with plane-wave basis sets[47] and at the B3LYP/LANL2DZ level.[50] However, a pair-potential ionic model predicted a structure similar to the C_2 structure to be slightly lower in energy than a structure similar to the (C_s **a**) structure.[23] The C_2 structure was the only structure obtained at the HF level[46] and at the B3P86/6-31G(d) level.[48] A structure similar to the C_1 structure was calculated to be the ground state using the SA-MCBH and B3LYP/DZVP approaches.[49]

3.1.4. Tetramer. The ground state of Ti_4O_8 is predicted to be $^1A_1$ in C_{2v} symmetry. A similar structure of C_{2h} symmetry

is calculated to be 5.2 kcal/mol higher in energy than the (C_{2v} **a**) structure at the CCSD(T)/aT//B3LYP/aD level. These two structures can be considered as two six-member rings with chair conformations fused together by sharing two titanium centers, and are different due to the relative orientation of the two rings. Flipping one of the titanium atoms with a terminal oxygen atom in the (C_{2v} **a**) structure will result in the (C_{2h} **a**) structure. A number of other structures were located for the tetramer. The (C_{2v} **b**) structure with a Ti_4O_6 unit similar to that of P_4O_6 and two terminal oxygen atoms lies 16.0 kcal/mol higher in energy than the (C_{2v} **a**) structure at the CCSD(T)/aT//B3LYP/aD level. This structure can be viewed as formed by pulling the tetra-bridge oxygen atom away from the titanium centers without terminal oxygen atoms in the (C_{2v} **a**) structure. The (C_{2h} **b**) structure formed by stacking two dimers with *trans* configurations in parallel lies higher in energy than the (C_{2v} **a**) structure by 11.7 kcal/mol at the B3LYP/aD level and 21.9 kcal/mol at the CCSD(T)/aT//B3LYP/aD level. The (C_{2v} **c**) structure, which is similar to the (C_{2h} **b**) structure, lies higher in energy than the (C_{2v} **a**) structure by 23.4 kcal/mol at the B3LYP/aD level and by 32.7 kcal/mol at the CCSD(T)/aT//B3LYP/aD level. The T_d structure with a cubic Ti_4O_4 unit and four terminal oxygen atoms lies higher in energy than the (C_{2v} **a**) structure by 28.4 kcal/mol at the B3LYP/aD level and by 24.2 kcal/mol at the CCSD(T)/aT//B3LYP/aD level. The D_{2d} structure with an eight-member ring and four terminal oxygen atoms lies higher in energy than the (C_{2v} **a**) structure by 57.0 kcal/mol at the B3LYP/aD level. The (C_{2v} **a**) structure has been predicted to be the ground state of the tetramer using the SA-MCBH and B3LYP/DZVP approaches.[49] However, a linear structure was predicted to be the ground state of the tetramer at the B3P86/6-31G(d) level,[48] which should lie much higher in energy on the basis of our calculations for the trimer. The (C_{2v} **b**) structure was predicted to be the ground state of the tetramer at the B3LYP/LANL2DZ level.[50]

3.2. Equilibrium Geometries of Anionic Clusters. ***3.2.1. Monomer.*** The ground state of TiO_2^- is calculated to be $^2A_1$ in C_{2v} symmetry. The O═Ti═O bond angle in the anion was estimated to be 128 ± 5° with matrix IR spectroscopy,[19] much larger than our calculated value of 114.3° at the CCSD(T)/aT level. The calculated Ti═O bond length for TiO_2^- at the CCSD(T)/aT level is 1.696 Å, 0.03 Å longer than that in the neutral. In their PES studies on TiO_2^-,[25] Wu and Wang concluded that there can be only a slight change in the Ti═O bond length between TiO_2^- and TiO_2 and the ground state of TiO_2^- should also have C_{2v} symmetry, as their vibrationally resolved spectrum shows only a very short Ti═O stretching progression. This is consistent with the conclusion reached by Chertihin and Andrews[19] on the basis of their calculations that their experimental estimate of the O═Ti═O bond angle in the anion of 128 ± 5° from matrix IR spectroscopy is too large. This is further confirmed by comparing our Franck−Condon simulations for the PES of TiO_2^- with the experiment as described in the next section.

3.2.2. Dimer. The ground state of $Ti_2O_4^-$ is predicted to be $^2A_1$ in C_{2v} symmetry at the CCSD(T)/CBS level. The ^2A_g state of C_{2h} symmetry is calculated to have one imaginary frequency of 164 cm^{-1} at the B3LYP/aD level. The $^2A'$ state of C_s symmetry is calculated to have no imaginary frequency at the B3LYP/aD level. It is predicted to be lower in energy than the ^2A_g state by ~0.1 kcal/mol without ZPE corrections, but higher in energy by ~0.3 kcal/mol with ZPE corrections. At the CCSD(T)/aD//B3LYP/aD level, the $^2A'$ state is calculated to be lower in energy than the ^2A_g state by ~0.2 kcal/mol without ZPE corrections, but higher in energy by ~0.2 kcal/mol with ZPE corrections. At the BP86/aD and PW91/aD levels, the ^2A_g state is calculated to have no imaginary frequency. Thus, the imaginary frequency calculated at the B3LYP/aD level for the ^2A_g state of $Ti_2O_4^-$ is very likely due to artificial symmetry breaking. Hybrid functionals have been found to be more prone to artificial symmetry breaking than pure functionals.[101,102] Artificial symmetry breaking has also been found in our previous calculations on the ground state of $M_2O_6^-$ (M = Cr, Mo, W), where the B3LYP/aD calculations yielded one imaginary frequency of 793, 233, and 141 cm^{-1}, respectively, and the BP86/aD calculations yielded no imaginary frequency.[38] Hereafter, we consider only the ^2A_g state.

At the CCSD(T)/CBS level, the ^2A_g state of C_{2h} symmetry is predicted to be only 1.6 kcal/mol higher in energy than the $^2A_1$ state of C_{2v} symmetry, and the $^2A_1$ state of C_{3v} symmetry is predicted to be 6.7 kcal/mol higher in energy than the $^2A_1$ state of C_{2v} symmetry. The (C_{2v} **b**) and (C_{2v} **c**) structures of $Ti_2O_4^-$ are predicted to be 28.6 and 135.5 kcal/mol higher in energy than the (C_{2v} **a**) structure respectively at the B3LYP/aD level. In contrast, Albaret et al. predicted the C_{3v} structure of $Ti_2O_4^-$ to be ~0.5 kcal/mol lower in energy than the C_{2h} structure at the LSDA level with plane-wave basis sets,[47] and Qu and Kroes predicted the C_{2h} structure to be the ground state of $Ti_2O_4^-$ at the B3LYP/LANL2DZ level.[50] The (C_{2v} **a**) structure of $Ti_2O_4^-$ has never been predicted before. In fact, Qu and Kroes obtained the C_{2h} structure when trying to optimize the (C_{2v} **a**) structure of $Ti_2O_4^-$.[50] In addition, artificial symmetry breaking is also likely to have occurred in Qu and Kroes' B3LYP calculation of the C_{2h} structure of $Ti_2O_4^-$, as they predicted it to have C_s symmetry.[50] Symmetry breaking did not occur in the LSDA calculation,[47] because the LSDA functional is less prone to this behavior than the B3LYP functional.[101,102]

The Ti═O bond lengths in the C_{2v} and C_{2h} structures of $Ti_2O_4^-$ are calculated to be ~0.04 Å longer than those in Ti_2O_4, and the Ti−O bond lengths are 0.01−0.03 Å longer. The most significant changes in the equilibrium geometries of these two structures are the O═Ti−O bond angles, which are calculated to be 116.9° and 114.9° in the neutral cluster, respectively, and 125.1° and 129.1° in the anion. In contrast, the changes in the O−Ti−O framework bond angles are less than 3°. For the C_{3v} structure, the Ti═O bond length is longer than that in the neutral by ~0.05 Å, the longer Ti−O bond lengths are shortened by ~0.03 Å, and the shorter ones are elongated by ~0.06 Å, which leads to Ti−O bond lengths that are closer to each other.

3.2.3. Trimer. The ground state of $Ti_3O_6^-$ is predicted to be $^2A'$ in C_s symmetry. The ^2B state of C_2 symmetry is calculated to have one imaginary frequency of 373 cm^{-1} at the B3LYP/aD level. However, at the BP86/aD and PW91/aD levels, the ^2B state is again calculated to have no imaginary frequency. Thus, artificial symmetry breaking is likely occurring for this structure at the B3LYP/aD level as well. The C_2 structure is calculated to be higher in energy than the (C_s a) structure by 40.2 kcal/mol at the CCSD(T)/aT//B3LYP/aD level. Optimization of the anion geometry starting from the C_1 structure of the neutral gives the same structure as that starting from the (C_s a) structure of the neutral. Optimization for the anion starting from the (C_s b) structure of the neutral gives the same structure as that starting from the C_{3v} structure of the neutral. The C_{3v} structure of $Ti_3O_6^-$ lies 33.6 kcal/mol higher in energy than the (C_s a) structure at the B3LYP/aD level, and the C_{2v} structure lies 69.7 kcal/mol higher in energy. The (C_s a) structure has been predicted to be the ground-state structure of $Ti_3O_6^-$ by

Albaret et al. at the LSDA level with plane-wave basis sets[47] and by Qu and Kroes at the B3LYP/LANL2DZ level.[50]

3.2.4. Tetramer. The ground state of $Ti_4O_8^-$ is predicted to be ^2A_g for the (C_{2h} **a**) structure at the CCSD(T)/aT//B3LYP/aD level. The (C_{2v} **a**) and (C_{2v} **b**) structures are predicted to be only 0.2 and 0.8 kcal/mol higher in energy than the (C_{2h} **a**) structure at the CCSD(T)/aT//B3LYP/aD level. At the B3LYP/aD level, both the ^2A_g state of the (C_{2h} **a**) structure and the $^2A_1$ state of the (C_{2v} **a**) structure have one imaginary frequency, 381 and 304 cm^{-1}, respectively, but no imaginary frequency is predicted at the BP86/aD and PW91/aD levels for these two states. At the B3LYP/aD level, the D_{2d}, (C_{2h} **b**), (C_{2v} **c**), and (C_{2v} **d**) structures lie 15.1, 17.8, 20.3, and 59.4 kcal/mol higher in energy than the (C_{2v} **b**) structure. The $^2A_1$ state of the D_{2d} structure and the ^2A_g state of the (C_{2h} **b**) structure have one imaginary frequency of 23i and 251i cm^{-1}, respectively, at the B3LYP/aD level. No imaginary frequency for these two structures is calculated at the BP86/aD and PW91/aD levels. The (C_{2v} **b**) structure has been predicted to be the ground state of $Ti_4O_8^-$ by Qu and Kroes at the B3LYP/LANL2DZ level.[50]

3.3. Computational Method Dependence of Geometries and Relative Energies. The titanium−oxygen bond lengths calculated at the CCSD(T)/aD level are in general slightly longer (less than 0.01 Å) than those calculated at the CCSD(T)/aT level. The calculated bond angles at the CCSD(T)/aD level are within 1° from those at the CCSD(T)/aT level. Similar observations have been made for the M_nO_{3n} (M = Cr, Mo, W; n = 1, 2) clusters and their anions.[38] For most of the species, the bond lengths calculated at the B3LYP/aD level are slightly shorter by ∼0.02 Å than those calculated at the CCSD(T)/aT level, whereas those calculated at the BP86/aD and PW91/aD levels are close to each other and are slightly shorter than those at the CCSD(T)/aT level by ∼0.01 Å. For most of the calculated bond angles, the B3LYP/aD results are within 1° of those calculated at the CCSD(T)/aT level, whereas the BP86/aD and PW91/aD values are again close to each other and are smaller than the CCSD(T)/aT values by up to 3°. For the ^2A_g state of $Ti_2O_4^-$, however, the calculated O═Ti−O bond angles at the B3LYP/aD level are smaller than the CCSD(T)/aT values by ∼3°, and those calculated at the BP86/aD and PW91/aD levels are smaller by ∼7°.

For the calculated relative energies of the dimer at the CCSD(T) level, the basis set extrapolation effect and core−valence correction can have a geometry dependence, but these effects are fairly small, <2 kcal/mol. For example, the basis set extrapolation and core−valence effects change the energy difference between the (C_{2v} **a**) and C_{2h} structures by <0.05 and <0.25 kcal/mol, respectively, whereas they stabilize the C_{3v} structure by 1.15−1.35 and 1.00−1.45 kcal/mol. The ZPE effect is slightly larger than the scalar relativistic effect, although both of them are less significant than the basis set extrapolation and core−valence effects. In addition, the basis set extrapolation effect from aT to CBS on the calculated relative energies of the dimer is <0.25 kcal/mol. Thus, the relative energies calculated at CCSD(T)/aT level with the core−valence and ZPE corrections are very close to the corrected CCSD(T)/CBS relative energies. For similar structures, the relative energies calculated at the CCSD(T)/aD level with just the ZPE correction are sufficiently close to the corrected CCSD(T)/CBS relative energies.

The calculated energy differences between the low-lying energy conformers of Ti_2O_4 at the B3LYP/aT//B3LYP/aD, BP86/aT//BP86/aD, and PW91/aT//PW91/aD levels are within 1 kcal/mol from the CCSD(T)/CBS results, except for the energy difference between the C_{3v} and C_{2h} structures at the B3LYP/aT//B3LYP/aD level, which is overestimated by ∼2 kcal/mol. For Ti_3O_6, the energy difference between the (C_s **a**) and C_2 structures is underestimated by these DFT methods by 6−8 kcal/mol as compared to that calculated at the CCSD(T)/aT//B3LYP/aD level. For Ti_4O_8, the energy differences between the (C_{2v} **a**) and (C_{2h} **a**) structures calculated with these DFT methods are within 1 kcal/mol from that calculated at the CCSD(T)/aT//B3LYP/aD level, but the energy differences between the (C_{2v} **a**) and (C_{2v} **b**) structures are underestimated by these DFT methods by 6−8 kcal/mol.

For $Ti_2O_4^-$, the (C_{2v} **a**) structure is predicted to be lower in energy than the C_{2h} structure by 1.6 kcal/mol at the CCSD(T)/CBS level. Although the C_{2v} structure is also predicted to be the ground state of $Ti_2O_4^-$ at the B3LYP/aT//B3LYP/aD level, the energy difference between these two structures is much smaller than that calculated at the CCSD(T)/CBS level, and the (C_{2v} **a**) and C_{2h} structures are predicted to be essentially isoenergetic. The BP86/aT//BP86/aD and PW91/aT//PW91/aD methods predict the C_{2h} structure to be the ground state of $Ti_2O_4^-$, although the calculated energy differences between the (C_{2v} **a**) and C_{2h} structures are again very small. Nevertheless, all these methods predict the C_{3v} structure to be higher in energy than the (C_{2v} **a**) structure by ∼7 kcal/mol. For $Ti_3O_6^-$, the energy difference between the (C_s **a**) and C_2 structures is underestimated by these DFT methods by 10−19 kcal/mol as compared to that calculated at the CCSD(T)/aT//B3LYP/aD level. For $Ti_4O_8^-$, the (C_{2h} **a**) structure is calculated to be the ground state at the CCSD(T)/aT//B3LYP/aD level, although the (C_{2v} **a**) and (C_{2v} **b**) structures are predicted to be only 0.2 and 0.8 kcal/mol higher in energy than the (C_{2h} **a**) structure. In contrast, the (C_{2v} **b**) structure is calculated to be ∼5 kcal/mol lower in energy than the (C_{2h} **a**) and (C_{2v} **a**) structures with these DFT methods, which are predicted to be nearly isoenergetic. This is consistent with the prediction of the (C_{2v} **b**) structure as the ground state of $Ti_4O_8^-$ by Qu and Kroes at the B3LYP/LANL2DZ level.[50]

The T_1 diagnostics from the CCSD(T) calculations for these neutral and anionic clusters range from 0.035 to 0.045, and are slightly larger for the smaller clusters than for the larger clusters. These values are similar to those for the M_3O_{3n} (M = Mo and W; n = 1−3) clusters and their anions, but smaller than those for M = Cr.[38,103]

3.4. Structural Evolution. The ground-state structures of the $(TiO_2)_n$ (n = 1−4) clusters are calculated to be the C_{2v} structure for n = 1, the (C_{2h} **a**) structure for n = 2, the (C_s **a**) structure for n = 3, and the (C_{2v} **a**) structure for n = 4, as shown in Figure 1. For these structures, each titanium center is surrounded by at most four oxygen atoms. This differs from the bulk structure, where each titanium center is surrounded by six oxygen atoms in a distorted octahedral configuration.[8,13] All of these structures have only two terminal oxygen atoms. All but one of the bridge oxygen atoms in the trimer and tetramer are bonded with two titanium centers. This again differs from the bulk structure, where each oxygen atom is surrounded by three titanium centers.[8,13] For the trimer, one of the bridge oxygen atoms is bonded with three titanium centers, with the bond lengths being 1.806, 2.088, and 2.088 Å calculated at the B3LYP/aD level. In comparison, these bond lengths in the rutile phase are 1.947, 1.947, and 1.982 Å,[8] and those in the anatase phase are 1.934, 1.934, and 1.980 Å.[13] For the tetramer, one of the bridge oxygen atoms is bonded with four titanium centers, and this type of oxygen atoms is not observed in any of the three natural phases.

TABLE 3: Energy Components of Electron Detachment Energies (ADEs/VDEs, eV) of $(TiO_2)_n^-$ ($n = 1-4$) to the Ground States of the Neutral Clusters for the Low-Lying Structures Calculated at the CCSD(T) Level and Compared with the Experimental Values

anion	transition	ΔE_{aD}[a]	ΔE_{aT}[b]	ΔE_{aQ}[b]	ΔE_{CBS}[c]	$\Delta E_{CV(D)}$[b,d]	$\Delta E_{CV(T)}$[b,e]	ΔE_{SR}[b,f]	ΔE_{ZPE}[g]	ΔE_{total}[h]	expt[i]
						ADEs					
TiO_2^-	$^2A_1 \rightarrow {}^1A_1$ (C_{2v})	1.605	1.604	1.607	1.609	+0.081	+0.049	−0.007	+0.007	1.66	1.59(3)
$Ti_2O_4^-$	$^2A_1 \rightarrow {}^1A_1$ (C_{2v} **a**)	1.870	1.857	1.860	1.862	+0.098	+0.062	−0.007	+0.036	1.95	2.06(5)
	$^2A_g \rightarrow {}^1A_g$ (C_{2h})	1.574	1.549	1.557	1.563	+0.083	+0.043	−0.005	+0.043	1.64	
	$^2A_1 \rightarrow {}^1A_1$ (C_{3v})	1.900	1.885	1.893	1.899	+0.090	+0.069	−0.001	+0.014	1.98	
$Ti_3O_6^-$	$^2A' \rightarrow {}^1A'$ (C_s **a**)	2.762	2.750			+0.109		+0.002	+0.016	2.88	2.78(10)
	$^2B \rightarrow {}^1A$ (C_2)	1.648	1.626			+0.082		−0.006	+0.045	1.75	
$Ti_4O_8^-$	$^2A_g \rightarrow {}^1A_g$ (C_{2h} **a**)	2.631	2.661			+0.073			+0.034	2.77	3.00(15)
	$^2A_1 \rightarrow {}^1A_1$ (C_{2v} **a**)	2.382	2.407			+0.084			+0.043	2.53	
	$^2A_1 \rightarrow {}^1A_1$ (C_{2v} **b**)	3.041	3.044			+0.142			+0.021	3.21	
						VDEs					
TiO_2^-	$^2A_1 \rightarrow {}^1A_1$ (C_{2v})	1.642	1.642	1.649	1.654	+0.088	+0.075	−0.006		1.72	1.59(3)
$Ti_2O_4^-$	$^2A_1 \rightarrow {}^1A_1$ (C_{2v} **a**)	2.188	2.199	2.210	2.218	+0.100	+0.103	−0.004		2.32	2.27(5)
	$^2A_g \rightarrow {}^1A_g$ (C_{2h})	2.127	2.073	2.087	2.099	+0.102	+0.120	−0.001		2.22	
	$^2A_1 \rightarrow {}^1A_1$ (C_{3v})	2.030	2.018	2.032	2.042	+0.083	+0.083	0.000		2.13	
$Ti_3O_6^-$	$^2A' \rightarrow {}^1A'$ (C_s **a**)	3.072	3.098			+0.093		+0.004		3.20	3.15(5)
	$^2B \rightarrow {}^1A$ (C_2)	1.684	1.709			+0.104		−0.003		1.81	
$Ti_4O_8^-$	$^2A_g \rightarrow {}^1A_g$ (C_{2h} **a**)	3.288	3.363			+0.043				3.41	3.65(5)
	$^2A_1 \rightarrow {}^1A_1$ (C_{2v} **a**)	3.174	3.241			+0.046				3.29	
	$^2A_1 \rightarrow {}^1A_1$ (C_{2v} **b**)	3.605	3.648			+0.102				3.75	

[a] Geometries from CCSD(T)/aD for $n = 1$ and 2, and from B3LYP/aD for $n = 3$ and 4. [b] Geometries from CCSD(T)/aT for $n = 1$ and 2, and from B3LYP/aD for $n = 3$ and 4. [c] Extrapolated using the mixed Gaussian/exponential formula for the CCSD(T) energies with the aD, aT, and aQ basis sets. [d] CCSD(T)/awCVDZ. [e] CCSD(T)/awCVTZ. [f] CISD/aT. [g] BP86/aD. [h] $\Delta E_{total} = \Delta E_{CBS} + \Delta E_{CV(T)} + \Delta E_{SR} + \Delta E_{ZPE}$ for $n = 1$ and 2, $\Delta E_{aT} + \Delta E_{CV(D)} + \Delta E_{SR} + \Delta E_{ZPE}$ for $n = 3$ and 4. [i] Reference 26.

A common feature among the calculated structures is the presence of two bridge oxygen atoms between each pair of adjacent titanium centers. This is very similar to that in the anatase phase, where each titanium center is surrounded by four closest titanium centers, and between each pair of these titanium centers, there are two bridge oxygen atoms.[13] In the rutile phase, there are only two pairs of such titanium centers.[8] For the other eight titanium centers with longer distances, only one bridge oxygen is shared between each pair. The fact that the structures of these small clusters are closer to that of the anatase phase is consistent with the experimental and theoretical predictions that the anatase phase is more stable than the rutile phase when the particle size is below ~14 nm.[14,15]

Our previous studies of the $(MO_3)_n$ (M = Cr, Mo, W; $n = 1-6$) clusters show that the ground states of these clusters have ring structures for $n > 2$ except for W_6O_{18}, which has a more stable cage structure.[96] For the $(TiO_2)_n$ ($n = 1-4$) clusters and their anions, however, the ground-state structures appear to be rather unique for each cluster size. Moreover, the ground-state structure of the anion can be different from that of the neutral, as found for the dimer and tetramer. The dimer and tetramer have more low-lying structures than the monomer and trimer. For the anions, nearly degenerate structures are found for the dimer and tetramer, but not for the monomer and trimer. The near-degeneracy in the anion in the dimer and tetramer of the titanium dioxide is different from that for the trimer of the molybdenum and tungsten trioxide[103] in that the former results from structural degeneracy and the latter results from orbital degeneracy. The subtle difference between these nearly degenerate structures causes the DFT methods to predict different ground-state structures as compared to the CCSD(T) method. To determine the correct ground-state structure, extended basis sets have to be used in the CCSD(T) calculations, and the core−valence corrections have to be included.

The structural difference between these titanium oxide clusters and the group VIB metal oxide clusters is most likely due to the fact that the former have fewer oxygen atoms and thus tend to form more compact structures by having more bridge oxygens as well as to the fact that the metal is formally in the +4 oxidation state for Ti and in the +6 oxidation state for the group VIB metals. For the ground states of the group VIB metal oxide clusters for $n = 2-5$, 2/3 of the oxygen atoms are terminal oxygen atoms,[96] whereas for the ground states of Ti_2O_4, Ti_3O_6 and Ti_4O_8, $^1/_2$, $^1/_3$ and $^1/_4$ of the oxygen atoms are terminal oxygen atoms, respectively. In addition, all bridge oxygen atoms are shared by two metal atoms for the group VIB metal oxide clusters,[96] whereas in Ti_3O_6 and Ti_4O_8, bridge oxygen atoms shared by three and four Ti atoms respectively, are found in their ground state structures.

3.5. Electron Detachment Energies. Table 3 lists the calculated ADEs and VDEs at the CCSD(T) level for the ground state of TiO_2^- and the low-lying states of $(TiO_2)_n^-$ ($n = 2-4$). Different contributions to these energies are also listed to provide insight into the potential sources of error, as such information is critical when applying the CCSD(T) method to larger clusters.

3.5.1. Monomer. For TiO_2^-, the calculated ADE and VDE at the CCSD(T)/CBS level including all the corrections are 1.66 and 1.72 eV, respectively. The experimental values for the ADE and VDE measured by Wang and co-workers are both 1.59(3) eV, as the 0−0 transition in the vibrationally resolved PES is also the strongest transition. Figure 4 shows the simulated spectra at the CCSD(T)/aT and BP86/aD levels, where the 0−0 transition is shifted to the experimental ADE. Both simulations are in good agreement with the experimental spectrum, and the short vibrational progression observed in the PES is assigned to the Ti=O symmetric stretch. The frequency of this vibration is predicted to be 968 and 988 cm^{-1} at the CCSD(T)/aT and BP86/aD levels, in excellent agreement with the experimental frequency of 960(40) cm^{-1}. It is calculated to be 1026 cm^{-1} at the B3LYP/aD level, which is too large as compared to the experimental and CCSD(T) values. The good agreement between the experimental and simulated spectra confirms the previous conclusion that there is little geometry change upon electron detachment.[25] The comparison between the experimen-

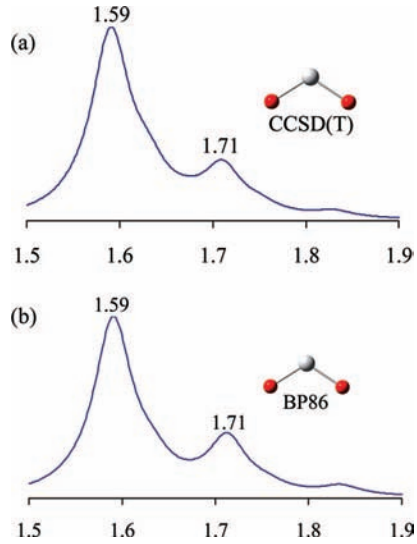

Figure 4. Simulated PES for TiO_2^- at the (a) CCSD(T)/aT and (b) BP86/aD levels. The 0−0 transitions are shifted to the experimental ADE. The transition energy is shown in electronvolts. The full width at half-maximum (fwhm) is 0.05 eV, and the vibrational temperature is 300 K.

tal and simulated spectra also indicates that when the 0−0 transition is the strongest transition, the center of the 0−0 band may be assigned to the ADE, but the VDE can be slightly higher in energy than the ADE depending on how strong the other bands are. Our calculated value for the ADE at the CCSD(T)/CBS level is within 0.07 eV (∼1.6 kcal/mol) of the experimental ADE and the error for the VDE on the basis of the above discussion should be similar.

3.5.2. Dimer. For $Ti_2O_4^-$, we calculated the ADEs and VDEs for the three lowest energy states, the $^2A_1$ states of the (C_{2v} **a**) and C_{3v} structures and the ^2A_g state of the C_{2h} structure. As the PES of $Ti_2O_4^-$ is not vibrationally resolved, the VDE is easier to locate than the ADE. Thus, we compare the VDEs first. The VDEs of the (C_{2v} **a**) and C_{2h} structures are calculated to be 2.32 and 2.22 eV at the CCSD(T)/CBS level, respectively. These values bracket and are in excellent agreement with the experimental value of 2.27(5) eV, and thus one cannot differentiate these two structures on the basis of the calculated VDEs. The VDE of the C_{3v} structure is calculated to be 2.13 eV, ∼0.1 eV lower than the experimental value. However, the C_{3v} structure of the anion is calculated to be 6.7 kcal/mol higher in energy than the (C_{2v} **a**) structure, and is not likely to be thermally populated under the experimental conditions. The ADEs of the (C_{2v} **a**) and C_{2h} structures are calculated to be 1.95 and 1.64 eV at the CCSD(T)/CBS level. The calculated ADE of the (C_{2v} **a**) structure is ∼0.1 eV lower than the experimental value of 2.06(5) eV, and that of the C_{2h} structure is ∼0.4 eV lower than the experimental value. The ADE of the C_{3v} structure is calculated to be 1.98 eV, which is within 0.1 eV of the experimental value. We note that in the PES obtained with 355 nm radiation, the signal starts to appear at ∼1.7 eV with a fairly sharp onset at ∼2.0 eV.[25] In the PES obtained with 266 nm radiation, the signal starts to appear at ∼1.0 eV, although it remains very weak until the onset at ∼2.0 eV.[25] For the PES obtained with 193 nm radiation, the signal starts to appear at ∼1.6 eV, and no noticeable signal appears to be present below this energy.[25] Thus, the signal observed in the PES at 266 nm below 1.7 eV may not be due to $Ti_2O_4^-$. In fact, it has been attributed to Ti_3O^-, as it has the same mass as $Ti_2O_4^-$,[25] although it is unclear whether Ti_3O^- has a signal at this energy range. The weak signal starting at ∼1.7 eV could be due to the C_{2h} structure on the basis of its calculated ADE of 1.66 eV at the CCSD(T)/CBS level. The C_{2h} structure of $Ti_2O_4^-$ is calculated to be ∼1.6 kcal/mol higher in energy than the (C_{2v} **a**) structure at the CCSD(T)/CBS level, and thus its thermal population is expected to be quite low, ∼7% at room temperature, resulting in much weaker intensity. Alternatively, the weak signal starting at ∼1.7 eV may be due to the transition from the (C_{2v} **a**) structure of $Ti_2O_4^-$ to the C_{2h} structure of Ti_2O_4, which has an ADE of 1.73 eV. However, this would result in large geometry changes and the Franck−Condon overlap is expected to be much smaller than the vertical transition. Another possibility for the weak signal starting at ∼1.7 eV is transitions from vibrationally excited states of the anionic (C_{2v} **a**) structure, as the vibrational temperature is quite high in the PES experiment of Wang and co-workers.[25]

For the calculated ADEs and VDEs at the CCSD(T) level for the monomer and dimer, the basis set extrapolation effect from the aD basis set is ∼0.01 eV except for the (C_{2v} **a**) and C_{2h} structures of the dimer, where it is ∼0.03 eV. In most cases, the basis set extrapolation effect is to slightly decrease the ADEs, and increase the VDEs except for the ADE of the monomer and the VDE of the C_{2h} structure of the dimer. The core−valence effect is more pronounced than the basis set extrapolation effect for the ADEs and VDEs of the monomer and dimer. The core−valence effect is to increase the ADEs by 0.04−0.07 eV, and to increase the VDE by 0.07−0.12 eV; its size is larger for the dimer than for the monomer. The core−valence corrections calculated at the CCSD(T)/awCVDZ level are 0.02−0.04 eV larger than those calculated at the CCSD(T)/awCVTZ level for the ADEs and are within 0.02 eV from those calculated at the CCSD(T)/awCVTZ level for the VDEs. The scalar relativistic effect is very small, less than 0.01 eV. Thus, the ADEs and VDEs calculated at the CCSD(T)/aD level with the core−valence corrections included are close to the corrected CCSD(T)/CBS values.

3.5.3 Trimer. For $Ti_3O_6^-$, we calculated the ADEs and VDEs for the $^2A'$ state of the (C_s **a**) structure and the ^2B states of the C_2 structure. We note that the C_2 structure is calculated to be higher in energy than the (C_s **a**) structure by 41.2 kcal/mol at the CCSD(T)/aT//B3LYP/aD level. The VDE of the (C_s **a**) structure is calculated to be 3.19 eV at the CCSD(T)/aT//B3LYP/aD level, in excellent agreement with the experimental value of 3.15(5) eV. The ADE is calculated to be 2.88 eV at the CCSD(T)/aT//B3LYP/aD level, again in excellent agreement with the experimental value of 2.78(10) eV. For the C_2 structure, the VDE is calculated to be 1.81 eV at the CCSD(T)/aT//B3LYP/aD level, ∼1.3 eV lower than the experimental value. Similarly, its ADE is calculated to be ∼1.75 eV at the CCSD(T)/aT//B3LYP/aD level, ∼1.0 eV lower than the experimental value. The much better agreement for the (C_s **a**) structure with the experiment than for the C_2 structure clearly confirms the assignment of the (C_s **a**) structure as the ground-state structure of $Ti_3O_6^-$.

3.5.4. Tetramer. For $Ti_4O_8^-$, we calculated the ADEs and VDEs for the (C_{2h} **a**), (C_{2v} **a**), and (C_{2v} **b**) structures. The VDE for the (C_{2h} **a**) structure calculated at the CCSD(T)/aT//B3LYP/aD level is 3.41 eV, lower than the experimental value of 3.65(5) eV by ∼0.2 eV. The VDE for the (C_{2v} **a**) structure calculated at the CCSD(T)/aT//B3LYP/aD level is 3.29 eV, lower than the experimental value by ∼0.4 eV. The VDE for the (C_{2v} **b**) structure calculated at the CCSD(T)/aT//B3LYP/aD level is 3.75 eV, slightly higher than the experimental value by ∼0.1 eV. The ADE for the (C_{2h} **a**) structure calculated at the CCSD(T)/aT//B3LYP/aD level is 2.77 eV, lower than the experimental value of 3.00 (15) eV by ∼0.2 eV. The ADE for the (C_{2v} **a**)

structure calculated at the CCSD(T)/aT//B3LYP/aD level is 2.53 eV, lower than the experimental value by ~0.5 eV. The ADE for the (C_{2v} **b**) structure calculated at the CCSD(T)/aT//B3LYP/aD level is 3.21 eV, larger than the experimental value by ~0.2 eV. The better agreement between calculated and experimental ADEs and VDEs for the (C_{2h} **a**) and (C_{2v} **b**) structures suggests that these two structures are likely to be present in the experiment. However, as the (C_{2v} **a**) and (C_{2v} **b**) structures are predicted to be only 0.2 and 0.8 kcal/mol higher in energy than the (C_{2h} **a**) structure, all three structures are likely to contribute to the PES. In fact, in the PES obtained at 193 nm radiation, signal starts to appear at ~2.6 eV,[25] which is ~0.1 eV higher in energy than the calculated ADE of the (C_{2v} **a**) structure of 2.53 eV. This suggests that the (C_{2v} **a**) structure may also be present in the experiment, considering the large geometry change accompanying the photodetachment process. Furthermore, the PES taken by Wu and Wang[25] at 193 nm for $Ti_4O_8^-$ appears to be much broader than that taken by Zhai and Wang[26] at the same photon energy, due to the better cooling of the clusters in the latter experiment, which reduces the population of the higher energy structures. Alternatively, the weak signal starting at ~2.6 eV could be attributed to transitions from the (C_{2h} **a**) and (C_{2v} **b**) structure of $Ti_4O_8^-$ to the (C_{2v} **a**) structure of Ti_4O_8, which have ADEs of 2.54 and 2.52 eV. These transitions will have very large geometry changes, and thus will have very small Franck−Condon overlaps. Vibrational hot bands are also likely to contribute to the weak signal starting at ~2.6 eV.

3.5.5. Computational Method Dependence of Electron Detachment Energies. Table 4 compares the calculated ADEs and VDEs at the B3LYP/aT//B3LYP/aD, BP86/aT//BP86/aD, and PW91/aT//PW91/aD levels with the CCSD(T) and experimental values. The excellent agreement between the CCSD(T) and experimental ADEs and VDEs for the C_{2v} structure of TiO_2^-, the (C_{2v} **a**) structure of $Ti_2O_4^-$, the (C_s **a**) structure of $Ti_3O_6^-$, and the (C_{2h} **a**) and (C_{2v} **b**) structures of $Ti_4O_8^-$, establishes them as the ground states of these anions, although the structures do not correspond to the ground-state structures of the neutral clusters for the dimer and tetramer. The calculated VDEs for these states at the B3LYP/aT//B3LYP/aD level are ~0.2 eV too high for the monomer and dimer, ~0.4 eV too high for the trimer and the (C_{2v} **b**) structure of the tetramer, and ~0.1 eV too high for the (C_{2h} **a**) structure of the tetramer as compared to the experimental values. The VDEs calculated at the BP86/aT//BP86/aD and PW91/aT//PW91/aD levels are close to each other and are within ~0.1 eV from the experimental values except for the (C_{2v} **b**) structure of the tetramer, where the errors in the calculated values are 0.26 and 0.22 eV, respectively. For the calculated ADEs, the B3LYP/aT//B3LYP/aD values are 0.1−0.2 eV higher than the experiment for the monomer and dimer, and 0.3−0.4 eV higher for the trimer and the (C_{2v} **b**) structure of the tetramer. The B3LYP/aT//B3LYP/aD value for the VDE of the (C_{2h} **a**) structure of the tetramer is in excellent agreement with the experimental value. The ADEs calculated at the BP86/aT//BP86/aD and PW91/aT//PW91/aD levels are again close to each other and are within 0.1 eV from the experimental values except for the (C_{2v} **b**) structure of the tetramer, for which the calculated ADEs are higher than the experimental value by 0.36 and 0.32 eV, respectively.

3.6. Lowest Triplet Excited States of Neutral Clusters. Figure 5 presents the optimized structures of the first triplet excited states of the low-lying structures of the neutral clusters. These triplet states arise from the excitation of one electron in the highest occupied molecular orbital (HOMO) in the neutral cluster to its lowest unoccupied molecular orbital (LUMO).

TABLE 4: Electron Detachment Energies (ADEs/VDEs, eV) of $(TiO_2)_n^-$ ($n = 1-4$) to the Ground States of the Neutral for the Low-Lying Structures Calculated at the CCSD(T), B3LYP/aT//B3LYP/aD, BP86/aT//BP86/aD, and PW91/aT//PW91/aD Levels and Compared with the Experimental Values

		CCSD(T)[a,b]	B3LYP[a]	BP86	PW91	expt[c]
	ADEs					
TiO_2^-	$^2A_1 \rightarrow {}^1A_1$ (C_{2v})	1.66	1.74	1.67	1.61	1.59(3)
$Ti_2O_4^-$	$^2A_1 \rightarrow {}^1A_1$ (C_{2v} **a**)	1.95	2.12	2.10	2.04	2.06(5)
	$^2A_g \rightarrow {}^1A_g$ (C_{2h})	1.64	1.87	1.85	1.78	
	$^2A_1 \rightarrow {}^1A_1$ (C_{3v})	1.98	2.20	2.07	2.01	
$Ti_3O_6^-$	$^2A' \rightarrow {}^1A'$ (C_s **a**)	2.88	3.10	2.87	2.81	2.78(10)
	$^2B \rightarrow {}^1A$ (C_2)	1.75	2.15	2.22	2.16	
$Ti_4O_8^-$	$^2A_g \rightarrow {}^1A_g$ (C_{2h} **a**)	2.77	3.00	2.95	2.89	3.00(15)
	$^2A_1 \rightarrow {}^1A_1$ (C_{2v} **a**)	2.53	2.75	2.73	2.67	
	$^2A_1 \rightarrow {}^1A_1$ (C_{2v} **b**)	3.21	3.35	3.36	3.32	
	VDEs					
TiO_2^-	$^2A_1 \rightarrow {}^1A_1$ (C_{2v})	1.72	1.79	1.71	1.65	1.59(3)
$Ti_2O_4^-$	$^2A_1 \rightarrow {}^1A_1$ (C_{2v} **a**)	2.32	2.43	2.36	2.30	2.27(5)
	$^2A_g \rightarrow {}^1A_g$ (C_{2h})	2.22	2.26	2.11	2.04	
	$^2A_1 \rightarrow {}^1A_1$ (C_{3v})	2.13	2.45	2.24	2.19	
$Ti_3O_6^-$	$^2A' \rightarrow {}^1A'$ (C_s **a**)	3.20	3.55	3.18	3.13	3.15(5)
	$^2B \rightarrow {}^1A$ (C_2)	1.81	2.32	2.36	2.31	
$Ti_4O_8^-$	$^2A_g \rightarrow {}^1A_g$ (C_{2h} **a**)	3.41	3.75	3.61	3.56	3.65(5)
	$^2A_1 \rightarrow {}^1A_1$ (C_{2v} **a**)	3.29	3.62	3.52	3.46	
	$^2A_1 \rightarrow {}^1A_1$ (C_{2v} **b**)	3.75	4.05	3.91	3.87	

[a] ZPEs from BP86/aD. [b] CCSD(T)/CBS for $n = 1$ and 2, CCSD(T)/aT for $n = 3$ and 4. [c] Reference 26.

Table 5 lists the calculated ADEs and VDEs of the anions to these states at the CCSD(T) and DFT levels.

3.6.1. Monomer. The first triplet excited state of TiO_2 is calculated to be the $^3B_2$ state. At the B3LYP/aD level, this state has one imaginary frequency of 377i cm^{-1}, but at the BP86/aD and PW91/aD levels it has no imaginary frequency. Thus, artificial symmetry breaking may be occurring in the first triplet state of the neutral cluster at the B3LYP/aD level. The O═Ti═O bond angle in the $^3B_2$ state is calculated to be 98° at the B3LYP/aD level, which is ~15° smaller than that in its ground state. The Ti═O bond length in the $^3B_2$ state is calculated to be 1.700 Å at the B3LYP/aD level, which is ~0.06 Å longer than that in its ground state.

3.6.2. Dimer. The first triplet excited states of the (C_{2v} **a**), C_{2h}, and C_{3v} structures of Ti_2O_4 are calculated to be $^3B_1$, ^3B_g, and $^3A_2$, respectively. At the B3LYP/aD level, the $^3B_1$ and ^3B_g states have one imaginary frequency of 143i and 446i cm^{-1}, respectively, and the $^3A_2$ state has two imaginary frequencies, both of 199i cm^{-1}. At the BP86/aD and PW91/aD levels, the $^3B_1$ and $^3A_2$ states have no imaginary frequencies, but the ^3B_g state still has one imaginary frequency of 466i and 480i cm^{-1}, respectively. The $^3A''$ state with

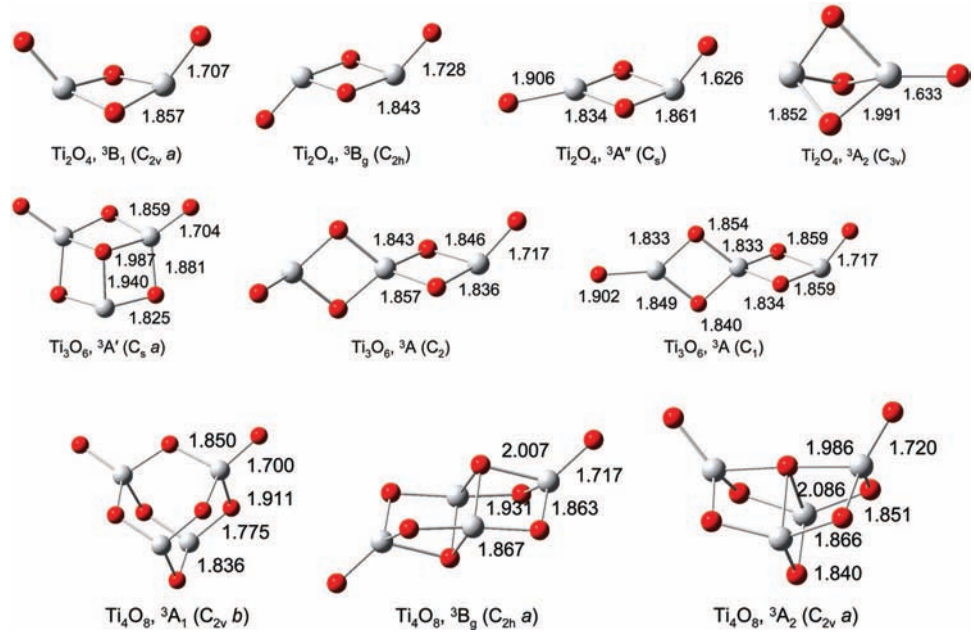

Figure 5. Structures of the first triplet excited states of $(TiO_2)_n$ ($n = 2-4$). The bond lengths (Å) shown are calculated at the B3LYP/aD level.

C_s symmetry derived from the ^3B_g state has no imaginary frequencies at the B3LYP/aD, BP86/aD, and PW91/aD levels. Without ZPE corrections, the $^3A''$ state is lower in energy than the ^3B_g state by 21.4, 3.9, and 3.8 kcal/mol at the B3LYP/aD, BP86/aD, and PW91/aD levels. At the CCSD(T)/aD//B3LYP/aD level, the $^3A''$ state is lower in energy than the ^3B_g state by 21.6 kcal/mol. At the B3LYP/aD level, the calculated Ti═O bond lengths in the $^3B_1$ state are 0.08 Å longer than those in the $^1A_1$ state of the (C_{2v} **a**) structure, whereas the Ti−O bond lengths are essentially the same in the singlet and triplet states. The O═Ti−O bond angles in the $^3B_1$ state are 5° larger than those in the singlet state, and the O−Ti−O bond angles are 2° larger. For the $^3A''$ state, one of the titanium-terminal oxygen bonds is significantly elongated by ∼0.3 Å from the ^1A_g state, and this terminal oxygen is nearly in the plane with the titanium and bridge oxygen atoms. The other bond lengths and bond angles in the $^3A''$ state differ from those in the ^1A_g state by less than 0.02 Å and 1°, respectively. For the $^3A_2$ state, the calculated Ti═O bond length at the B3LYP/aD level is nearly the same as that for the $^1A_1$ state of the C_{3v} structure, the longer Ti−O bonds are slightly shortened by ∼0.01 Å, the shorter Ti−O bonds are elongated by ∼0.08 Å, and the bond angles change by 2−3°.

3.6.3. Trimer. The first triplet excited states of the (C_s **a**) and C_2 structures of Ti_3O_6 are calculated to be the $^3A'$ and ^3A (C_2) state, respectively. At the B3LYP/aD level, both states have one imaginary frequency of 991i and 257i cm^{-1}, respectively. At the BP86/aD and PW91/aD levels, the $^3A'$ state has no imaginary frequencies, but the ^3A (C_2) state still has one imaginary frequency of 577i and 579i cm^{-1}, respectively. The ^3A state with C_1 symmetry derived from the ^3A (C_2) state is calculated to have no imaginary frequencies at the B3LYP/aD, BP86/aD, and PW91/aD levels. Without ZPE corrections, the ^3A (C_1) state is lower in energy than the ^3A (C_2) state by 27.8, 4.1, and 3.9 kcal/mol at the B3LYP/aD, BP86/aD, and PW91/aD levels. At the CCSD(T)/aD//B3LYP/aD level, the ^3A (C_1) state is lower in energy than the ^3A (C_2) state by 16.8 kcal/mol.

3.6.4. Tetramer. The first triplet excited states of the (C_{2v} **b**), (C_{2h} **a**) and (C_{2v} **a**) structures of Ti_4O_8 are calculated to be the $^3A_1$, ^3B_g, and $^3A_2$, respectively. At the B3LYP/aD level, the $^3A_1$ state has one imaginary frequency of 922i cm^{-1}, and the other two triplet states both have two imaginary frequencies. At the BP86/aD and PW91/aD levels, all these triplet states have no imaginary frequencies.

3.6.5. Triplet Electron Detachment Energies. For the VDEs to these triplet states (higher energy bands) starting from the anions, the CCSD(T)/aD//B3LYP/aD value is ∼0.1 eV higher than the experimental value for the monomer. For the dimer, the calculated VDE to the triplet state for the (C_{2v} **a**) structure is ∼0.2 eV lower than the experimental value, and that for the C_{2h} structure is in good agreement with experiment. For the trimer, the calculated VDE to the triplet state for the (C_s **a**) structure is ∼0.9 eV lower than the experimental value, which is inconsistent with the observation. This suggests that the experimental VDE for the excited state corresponds to a higher excited state than we calculated. For the tetramer, the calculated VDEs to the triplet state for the (C_{2h} **a**) and (C_{2v} **a**) structures are ∼0.2 eV lower than the experimental value, and that for the (C_{2v} **b**) structure is ∼1.0 eV lower than the experimental value.

For the calculated ADEs to the triplet states, the CCSD(T)/aD//B3LYP/aD value is in good agreement with the experimental value for the monomer. For the dimer, the calculated ADEs to the triplet states are ∼0.2 eV too high for the (C_{2v} **a**) structure and 0.4−0.6 eV too low for the C_{2h} and C_{3v} structures. For the trimer, the calculated ADEs to the triplet states are ∼0.3 eV too high for the (C_s **a**) structure and ∼0.9 eV too low for the C_2 structure. For the tetramer, the calculated ADEs are ∼0.4 eV too high for the (C_{2h} **a**) and (C_{2v} **a**) structures and ∼0.5 eV too low for the (C_{2v} **b**) structure. We note that the first excited-state band is not as well resolved in the PES for the trimer and tetramer as for the monomer and dimer.

The calculated ADEs and VDEs for the first triplet states at the B3LYP/aT//B3LYP/aD level are in general 0.2−0.4 eV lower than the CCSD(T)/aD values. For the dimer, the B3LYP/aT//B3LYP/aD and CCSD(T)/aD//B3LYP/aD values are nearly identical. For the ADE of the C_2 structure of the trimer, the B3LYP/aT//B3LYP/aD value is ∼0.1 eV higher than the CCSD(T)/aD//B3LYP/aD value. The calculated ADEs and VDEs for the first triplet states at the BP86/aT//BP86/aD and PW91/aT//PW91/aD levels are very close to each other, and they are in general smaller than the CCSD(T)/aD//B3LYP/

TABLE 5: Electron Detachment Energies (ADEs/VDEs, eV) of $(TiO_2)_n^-$ ($n = 1-4$) to the First Triplet Excited States of the Neutral for the Low-Lying Structures Calculated at the CCSD(T)/aD//B3LYP/aD, B3LYP/aT//B3LYP/aD, BP86/aT//BP86/aD, and PW91/aT//PW91/aD Levels and Compared with the Experimental Values

		CCSD(T)[a]	B3LYP[a]	BP86	PW91	expt[b]
	ADEs					
TiO_2^-	$^2A_1 \rightarrow {}^3B_2$ (C_{2v})	3.85	3.66	3.70	3.65	3.81(10)
$Ti_2O_4^-$	$^2A_1 \rightarrow {}^3B_1$ (C_{2v} **a**)	4.88	4.80	4.47	4.41	4.65(10)
	^2A_g (C_{2h}) $\rightarrow$ $^3A''$ (C_s)	4.10	4.10	4.54	4.49	
	$^2A_1 \rightarrow {}^3A_2$ (C_{3v})	4.22	4.22	4.29	4.24	
$Ti_3O_6^-$	$^2A' \rightarrow {}^3A'$ (C_s **a**)	5.37	5.15	4.90	4.85	5.04(10)
	^2B (C_2) $\rightarrow$ ^3A (C_1)	4.16	4.27	4.82	4.78	
$Ti_4O_8^-$	$^2A_g \rightarrow {}^3B_g$ (C_{2h} **a**)	5.98	5.65	5.16	5.11	5.60(15)
	$^2A_1 \rightarrow {}^3A_2$ (C_{2v} **a**)	5.95	5.61	5.16	5.12	
	$^2A_1 \rightarrow {}^3A_1$ (C_{2v} **b**)	5.08	4.93	4.63	4.59	
	VDEs					
TiO_2^-	$^2A_1 \rightarrow {}^3B_2$ (C_{2v})	4.01	3.78	3.81	3.76	3.90(3)
$Ti_2O_4^-$	$^2A_1 \rightarrow {}^3B_1$ (C_{2v} **a**)	5.10	5.08	4.73	4.68	5.30(10)
	$^2A_g \rightarrow {}^3B_g$ (C_{2h})	5.25	5.26	4.86	4.80	
	$^2A_1 \rightarrow {}^3A_2$ (C_{3v})	4.33	4.37	4.40	4.35	
$Ti_3O_6^-$	$^2A' \rightarrow {}^3A'$ (C_s **a**)	5.58	5.39	5.09	5.03	6.50(10)
	$^2B \rightarrow {}^3A$ (C_2)	5.10	5.65	5.13	5.08	
$Ti_4O_8^-$	$^2A_g \rightarrow {}^3B_g$ (C_{2h} **a**)	6.13	5.89	5.31	5.27	6.30(10)
	$^2A_1 \rightarrow {}^3A_2$ (C_{2v} **a**)	6.13	5.90	5.34	5.31	
	$^2A_1 \rightarrow {}^3A_1$ (C_{2v} **b**)	5.30	5.18	4.85	4.81	

[a] ZPEs from BP86/aD. [b] Reference 26. VDEs were estimated from the PES.

aD values by 0.2−0.6 eV. For the ADEs of the C_{2h} structure of the dimer and the C_2 structure of the trimer, the BP86/aT//BP86/aD and PW91/aT//PW91/aD values are 0.4−0.7 eV higher than the CCSD(T)/aD//B3LYP/aD values.

3.7. Reorganization Energies and Energy Gaps. Table 6 presents the calculated reorganization energies and energy gaps compared with the experimental values. The reorganization energy is calculated as the difference between the ADE and VDE for the ground state of the neutral cluster and is an energetic measure of the structural differences between the ground states of the neutral and the anionic clusters. The experimental reorganization energies increase from 0.00 eV for the monomer, to 0.21 eV for the dimer, to 0.37 eV for the trimer, to 0.65 eV for the tetramer. The calculated values at the DFT and CCSD(T) levels for the ground states of the anions are within 0.1 eV from the experimental values.

The experimental energy gap is defined as the ADE difference between the ground state and first excited state of the neutral and corresponds to the first excitation energy. This can be approximately calculated as the first triplet vertical excitation energy at the ground-state geometry of the neutral cluster at the TD-DFT level. The experimental energy gaps are ∼2.2 eV for the monomer and trimer and ∼2.6 eV for the dimer and tetramer. The first triplet vertical excitation energy calculated at the TD-DFT level is only slightly lower than the singlet vertical excitation energy, and in fact in many cases they are almost identical. This is very different from the $(MO_3)_n$ (M = Cr, Mo, W; $n = 1-6$) clusters, where the first triplet excitation energy is up to 0.4 eV lower than the first singlet excitation energy.[96] It is consistent with the previous prediction of near-degenerate singlet and triplet excited states for TiO_2.[32] In addition, the TD-DFT first singlet excitation energy of TiO_2 calculated at the BP86/aD level of 2.41 eV is in good agreement with the experimental value of 2.3 eV measured from the emission spectrum.[18]

The first triplet vertical excitation energies calculated at the TD-DFT level with the B3LYP functional are in general larger than the experimental energy gaps, by ∼0.2 eV for the monomer and ∼0.6 eV for the dimer and trimer. For the tetramer, the calculated values are 1.0−1.3 eV too high for the (C_{2h} **a**) and (C_{2v} **a**) structures, and ∼0.3 eV too low for the (C_{2v} **b**) structure. The BP86/aD and PW91/aD values differ from each other by up to 0.4 eV, with the BP86/aD values being larger in general. The energy gaps calculated at the BP86/aD level are larger than the experimental values by ∼0.1 eV for the monomer, ∼0.2 eV for the dimer, but smaller than the experimental value by ∼0.3 eV for the trimer. For the tetramer, the calculated energy gap of the (C_{2h} **a**) structure at the BP86/aD level is in excellent agreement with the experimental value, but that for the (C_{2v} **b**) structure is ∼1.3 eV lower and that for the (C_{2v} **a**) structure is ∼0.3 eV higher. For the PW91/aD method, the calculated values are smaller than experiment by ∼0.2 eV for the monomer and ∼0.4 eV by for the trimer. For the dimer and the (C_{2h} **a**) structure of the tetramer, the PW91/aD value is in good agreement with the experiment, whereas that for the (C_{2v} **b**) structure is ∼1.4 eV smaller and that for the (C_{2v} **a**) structure is ∼0.3 eV higher. Overall, the BP86 and PW91 functionals perform better than the B3LYP functional for the calculations of the excitation energies at the TD-DFT level. For the tetramer, the much better agreement for the BP86 and PW91 excitation energies with the experimental value for the (C_{2h} **a**) structure than the (C_{2v} **b**) structure is consistent with the fact that the (C_{2h} **a**) structure is predicted to be lower in energy than the (C_{2v} **b**) structure at the CCSD(T)/aT//B3LYP/aD level.

Table 7 shows the adiabatic energy gaps calculated as the energy difference between the first triplet excited state and the ground state of the neutral cluster at the CCSD(T) and DFT levels. For the monomer, the CCSD(T)/aD//B3LYP/aD value of 2.24 eV is in excellent agreement with the experimental value of 2.22 eV. For the dimer, the CCSD(T)/aD//B3LYP/aD values are larger than the experimental value by ∼0.4 eV for the (C_{2v} **a**) structure and smaller by 0.1−0.3 eV for the C_{2h} and C_{3v} structures. For the trimer, the CCSD(T)/aD//B3LYP/aD values are larger than the experimental value by 0.2−0.3 eV for the (C_s **a**) and C_2 structures. For the tetramer, the CCSD(T)/aD//B3LYP/aD values are larger than the experimental value by 0.7−0.9 eV for the (C_{2h} **a**) and (C_{2v} **a**) structures and smaller by ∼0.6 eV for the (C_{2v} **b**) structure. The adiabatic energy gaps calculated at the B3LYP/aT//B3LYP/aD level are smaller than the CCSD(T)/aD//B3LYP/aD values by 0.2−0.7 eV. At the BP86/aT//BP86/aD and PW91/aT//PW91/aD levels, the calculated adiabatic energy gaps are essentially identical, unlike the vertical energy gaps calculated at the TD-DFT levels. These values are lower than the CCSD(T)/aD values by 0.2−1.1 eV

TABLE 6: Calculated Reorganization Energies (ΔE_{reorg}, eV) and Vertical Energy Gaps (ΔE_{gap}, eV) for $(TiO_2)_n$ ($n = 1-4$) and Compared with Their Experimental Values

		ΔE_{reorg}[a]					ΔE_{gap}[b]						
		CCSD(T)[c]	B3LYP[d]	BP86[d]	PW91[d]	expt[e]	B3LYP(T)[f]	BP86(T)[f]	PW91(T)[f]	B3LYP(S)[g]	BP86(S)[g]	PW91 (S)[g]	expt[e]
TiO_2	$^1A_1$ (C_{2v})	0.06	0.05	0.04	0.04	0.00(3)	2.46	2.33	1.98	2.57	2.41	2.09	2.22(10)
Ti_2O_4	$^1A_1$ (C_{2v} **a**)	0.37	0.31	0.26	0.27	0.21(5)	3.19	2.80	2.59	3.26	2.86	2.65	2.59(10)
	^1A_g (C_{2h})	0.58	0.38	0.26	0.26		3.65	3.24	3.08	3.74	3.30	3.15	
	$^1A_1$ (C_{3v})	0.15	0.26	0.18	0.18		2.67	2.37	2.29	2.77	2.46	2.38	
Ti_3O_6	$^1A'$ (C_s **a**)	0.32	0.44	0.31	0.31	0.37(10)	2.91	1.95	1.81	2.93	1.97	1.82	2.26(10)
	^1A (C_2)	0.06	0.17	0.15	0.15		3.57	3.09	2.96	3.68	3.14	3.01	
Ti_4O_8	^1A_g (C_{2h} **a**)	0.64	0.75	0.66	0.67	0.65(15)	3.62	2.59	2.60	3.65	2.61	2.62	2.60(15)
	$^1A_1$ (C_{2v} **a**)	0.76	0.87	0.79	0.79		3.92	2.90	2.91	3.97	2.93	2.94	
	$^1A_1$ (C_{2v} **b**)	0.54	0.70	0.55	0.55		2.31	1.32	1.16	2.34	1.35	1.19	

[a] The reorganization energy is calculated as the difference between the ADE and VDE for the ground state of the neutral cluster. [b] The theoretical energy gap is calculated as the first excitation energy from the TD-DFT calculation with the aD basis set at the neutral ground-state geometry. The experimental energy gap is calculated as the difference between the ADEs for the ground state and the first excited state of the neutral cluster measured from the PES. [c] CCSD(T)/CBS for $n = 1$ and 2, and CCSD(T)/aT for $n = 3$ and 4. [d] Calculated with the aT basis set. [e] Reference 26. [f] The first triplet excitation energy. [g] The first singlet excitation energy.

TABLE 7: Calculated Adiabatic Energy Gaps (ΔE_{gap}, eV)[a] of $(TiO_2)_n$ ($n = 1-4$) at the CCSD(T)/aD//B3LYP/aD, B3LYP/aT//B3LYP/aD, BP86/aT//BP86/aD, PW91/aT//PW91/aD Levels

		CCSD(T)[b]	B3LYP[b]	BP86	PW91
TiO_2	$^1A_1 \rightarrow {}^3B_2$ (C_{2v})	2.24	1.92	2.03	2.04
Ti_2O_4	^1A_g (C_{2h})$\rightarrow$ $^3A''$ (C_s)	2.48	2.23	2.70	2.70
	$^1A_1 \rightarrow {}^3B_1$ (C_{2v} **a**)	2.97	2.68	2.38	2.37
	$^1A_1 \rightarrow {}^3A_2$ (C_{3v})	2.30	2.03	2.22	2.23
Ti_3O_6	$^1A' \rightarrow {}^3A'$ (C_s **a**)	2.59	2.05	2.03	2.03
	^1A (C_2) $\rightarrow {}^3A$ (C_1)	2.46	2.12	2.61	2.62
Ti_4O_8	$^1A_1 \rightarrow {}^3A_2$ (C_{2v} **a**)	3.53	2.86	2.43	2.44
	$^1A_g \rightarrow {}^3B_g$ (C_{2h} **a**)	3.32	2.65	2.21	2.22
	$^1A_1 \rightarrow {}^3A_1$ (C_{2v} **b**)	2.02	1.57	1.27	1.26

[a] The energy gap is calculated as the energy difference between the first triplet excited state and the ground state of the neutral cluster. [b] ZPEs from BP86/aD.

except for the C_{2h} structure of the dimer and the C_2 structure of the trimer, where they are higher by ~0.2 eV. Compared to the TD-DFT vertical excitation energies, the adiabatic energy gaps are smaller by 0.5−1.4 eV for the B3LYP functional, and up to 0.5 eV for the BP86 and PW91 functionals.

3.8. Electron Localization in the Anions. Previous work by Wang and co-workers[26] suggested that the extra electrons in the anions of the titanium clusters are localized, which was suggested to induce large geometry change upon photodetachment. Figure 6 shows the highest occupied molecular oribitals (HOMOs) of the neutral clusters, the singly occupied molecular orbitals (SOMOs) and the electron spin density of the anions. The HOMOs of the neutral clusters are of O 2pπ character. The 2pπ orbitals on both the bridge and terminal oxygen atoms can have significant contributions. The contributions from the 2pπ orbitals of the bridge and terminal oxygen atoms can be different for different structures. For example, for the C_{2h} and (C_{2v} **a**) structures of the dimer, the HOMOs have nearly equal contributions from the 2pπ orbitals on the bridge and terminal oxygen atoms, whereas for the C_{3v} structure of the dimer, the HOMO is dominated by the contributions from the bridge oxygen atoms only.

The lowest unoccupied molecular orbitals (LUMOs) of the neutral clusters (not shown) are similar to the SOMOs of the anions, which are dominated by the Ti $3d_{z^2}$ orbital in most cases. In addition, mixing with the Ti 4s orbital allows these SOMOs to hybridize and move the excess electron density away from the neighboring negatively charged oxygen atoms to reduce electron repulsion. For the monomer and the (C_{2v} **a**) and (C_{2h} **a**) structures of the tetramer, the Ti 3d orbital involved is not the $3d_{z^2}$ orbital. These Ti centers are bonded with two oxygen atoms for the monomer and four oxygen atoms for the (C_{2v} **a**) and (C_{2h} **a**) structures of the tetramer, in contrast to three oxygen atoms for the others. The electron spin density of the anions is consistent with their SOMOs. The electron spin density of the anions is equally distributed on two of the metal centers except for the monomer, the C_{3v} structure of the dimer, and the (C_s **a**) structure of the trimer. Thus, the extra electron in the anions is partially delocalized on two metal centers for the ground states of the dimer and tetramer, but localized on a single metal center for the monomer and trimer. Furthermore, for the C_{3v} structure of the dimer and the low-lying structures of the trimer and tetramer, the extra electron of the anions are located on the metal centers without terminal oxygen atoms to reduce electron repulsion.

One has to take care in predicting the ground states of the anions as well as the first triplet excited states of the neutral clusters with hybrid functionals, which can introduce symmetry breaking. As many previous studies have been done with hybrid functionals for the anions without addressing potential symmetry breaking issues, they predicted less symmetric structures to be

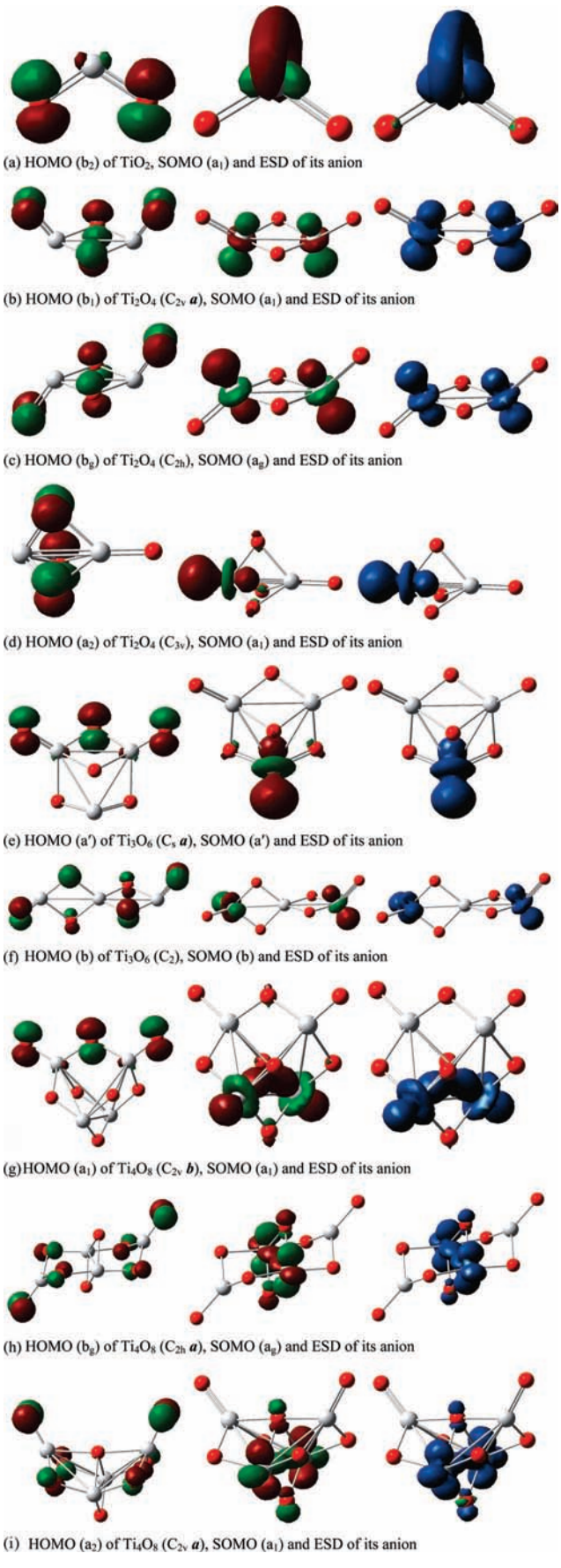

Figure 6. Highest occupied molecular orbital (HOMO) of $(TiO_2)_n$ ($n = 1-4$), the singly occupied molecular orbital (SOMO) and electron spin density (ESD) of their anions at the B3LYP/aD level.

the ground-state structures for the dimer and tetramer.[50] For these less symmetric structures, the extra electron is likely to be more or less localized on one of the titanium centers. However, the potential energy surfaces for these anions are very flat and the more symmetric structures have more delocalization so it is extremely difficult to ascertain how localized the electrons actually are.

Large structural changes are not necessarily caused by electron localization, and this is shown in the Franck−Condon simulations of the PES in Figure 7 for the dimer and trimer. For the anion of the dimer, the SOMOs of the (C_{2v} **a**) and C_{2h} structures are delocalized on both titanium centers, whereas that of the C_{3v} structure is localized on the titanium center without a terminal oxygen atom. However, our simulations show that the C_{3v} structure has the smallest geometry change upon electron detachment despite its electron localization. For the anion of the trimer, the SOMO of the (C_s **a**) structure is localized on the Ti atom without the terminal oxygen atom, whereas that of the C_2 structure is delocalized on two terminal Ti atoms. Our simulations show that the C_2 structure has only slightly less geometry change accompanying electron detachment than the (C_3 **a**) structure. For the tetramer, the Franck−Condon overlaps between the anion and that of the neutral cluster for all three low-lying structures are negligibly small, even though the extra electron in the anion is partially delocalized on two of the titanium centers. From these simulations and our simulations for the PES of the group VIB metal oxide clusters,[38,80] we found that larger structural changes are generally present in large clusters, resulting in broad spectra.

3.9. Clustering Energies. Table 8 presents the normalized and differential clustering energies at 0 K for the ground states of the $(TiO_2)_n$ ($n = 2-4$) clusters calculated at the CCSD(T) level. Those calculated at 0 K for the other low-lying structures and at 298 K in terms of the enthalpy and free energy are included in the Supporting Information. Different contributions to these energies are also listed to provide insight into their relative importance. The normalized clustering energy is the ratio of the energy required to completely break down the cluster to the monomer and the number of monomers in the cluster, and the differential clustering energy is the energy required to remove one monomer from the cluster.

The normalized clustering energies at 0 K for the ground states of the $(TiO_2)_n$ ($n = 2-4$) clusters range from 60 to 100 kcal/mol, increasing from the dimer to the tetramer. The normalized clustering enthalpies at 298 K are <0.5 kcal/mol larger than those at 0 K, whereas the normalized clustering free energies at 298 K are lower than those at 0 K by ∼6 kcal/mol for the dimer, ∼8 kcal/mol for the trimer, and ∼10 kcal/mol for the tetramer. The differential clustering energies at 0 K for the ground states of these clusters range from 120 to 140 kcal/mol, also increasing from the dimer to the tetramer. The differential clustering enthalpies at 298 K are greater than those at 0 K by ∼0.5 kcal/mol, whereas the differential clustering free energies at 298 K are lower than those at 0 K by 12−14 kcal/mol due to the formation of a free monomer on one side of the equation.

For the dimer, the normalized clustering energy is exactly half of the differential clustering energy, based on eqs 1 and 2. For the normalized clustering energies of the dimer, the CBS extrapolation effect from the aD basis set is ∼0.3 kcal/mol for the (C_{2v} **a**) and C_{2h} structures, and ∼0.9 kcal/mol for the C_{3v} structure. The CBS extrapolation effect from the aT basis is even smaller, 0.2−0.3 kcal/mol for all three conformers. The core−valence contributions calculated at the CCSD(T)/awCVTZ

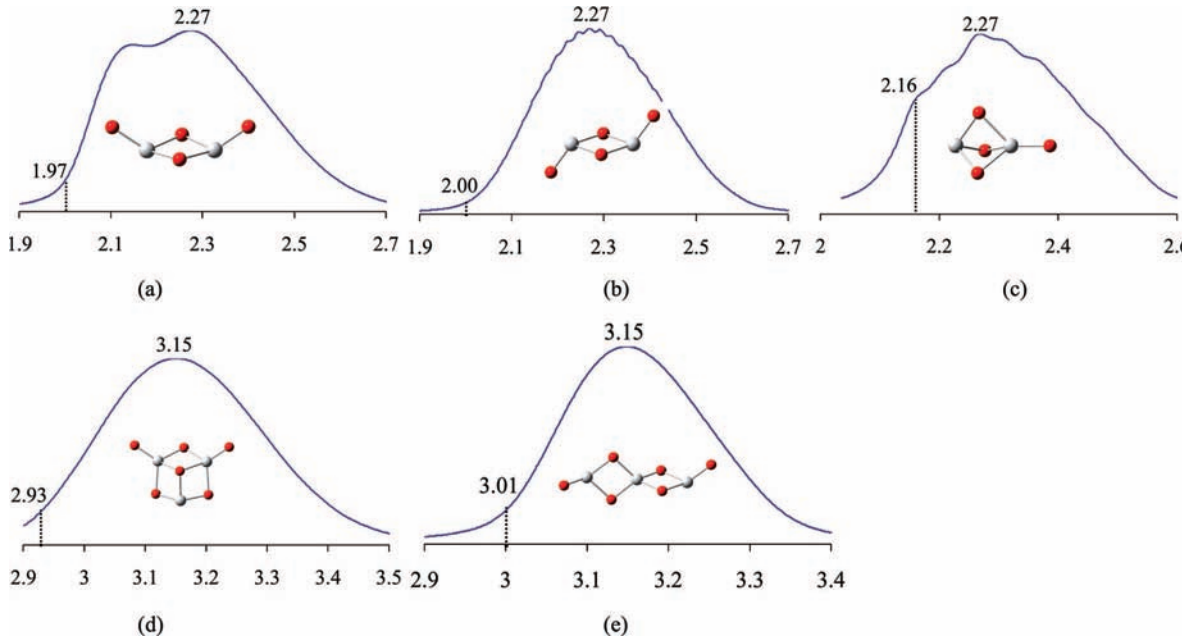

Figure 7. Simulated PES for $Ti_2O_4^-$ and $Ti_3O_6^-$ at the BP86/aD level. The peak maximum is shifted to the experimental VDE. The transition energy shown is in electronvolts. The full width at half-maximum (fwhm) is 0.05 eV, and the vibrational temperature is 300 K.

TABLE 8: Normalized and Differential Clustering Energies at 0 K (ΔE_{0K}, kcal/mol) for $(TiO_2)_n$ ($n = 2-4$) Calculated at the CCSD(T) Level

		ΔE_{aD}[a]	ΔE_{aT}[b]	ΔE_{aQ}[b]	ΔE_{CBS}[c]	$\Delta E_{CV(D)}$[b,d]	$\Delta E_{CV(T)}$[b,e]	ΔE_{SR}[b,f]	ΔE_{ZPE}[g]	ΔE_{0K}[h]
					Normalized					
Ti_2O_4	^1A_g (C_{2h})	60.69	60.85	60.96	61.03	+2.54	+1.60	−0.31	−1.08	61.2
Ti_3O_6	$^1A'$ (C_s **a**)	82.85	82.95			+3.84	-	−0.42	−1.34	85.0
Ti_4O_8	$^1A_1$ (C_{2v} **a**)	95.29	95.57			+4.79	-	−0.53	−1.48	98.4
					Differential					
Ti_2O_4	^1A_g (C_{2h})	121.38	121.70	121.92	122.05	+5.08	+3.20	−0.63	−2.16	122.5
Ti_3O_6	$^1A'$ (C_s **a**)	127.16	127.14	-	-	+6.44	-	−0.65	−1.85	131.1
Ti_4O_8	$^1A_1$ (C_{2v} **a**)	132.64	133.43	-	-	+7.65	-	−0.86	−1.92	138.3

[a] Geometries from CCSD(T)/aD for $n = 1$ and 2, and from B3LYP/aD for $n = 3$ and 4. [b] Geometries from CCSD(T)/aT for $n = 1$ and 2, and from B3LYP/aD for $n = 3$ and 4. [c] Extrapolated using the mixed Gaussian/exponential formula for the CCSD(T) energies with the aD, aT, and aQ basis sets. [d] CCSD(T)/awCVDZ. [e] CCSD(T)/awCVTZ. [f] CISD/aT. [g] BP86/aD. [h] $\Delta E_0 = \Delta E_{CBS} + \Delta E_{CV(T)} + \Delta E_{SR} + \Delta E_{ZPE}$ for $n = 1$ and 2, $\Delta E_{aT} + \Delta E_{CV(D)} + \Delta E_{SR} + \Delta E_{ZPE}$ for $n = 3$ and 4.

level are 1.5−1.6 kcal/mol for the (C_{2v} **a**) and C_{2h} structures, and ∼2.1 kcal/mol for the C_{3v} structure. The core−valence corrections are overestimated at the CCSD(T)/awCVDZ level by ∼1.0 kcal/mol for the (C_{2v} **a**) and C_{2h} structures, and by ∼1.4 kcal/mol for the C_{3v} structure. The core−valence contributions calculated at the CCSD(T)/wCVTZ level without the augmented functions are 0.2−0.3 kcal/mol lower than those calculated at the CCSD(T)/awCVTZ level. The scalar relativistic corrections are 0.3−0.4 kcal/mol, much smaller than the core−valence corrections, but close to the CBS corrections from the aT basis set. The ZPE corrections are 0.9−1.1 kcal/mol, again smaller than the core−valence corrections. Similar conclusions are drawn for the differential clustering energy of the dimer. The above observations indicate that the core−valence corrections are the most significant additional contribution to the clustering energies beyond the valence electronic energy.

For the trimer and tetramer, the differential clustering energy is related to its normalized clustering energy and the normalized clustering energy of the cluster with one less TiO_2 unit. For the normalized clustering energies of the trimer and tetramer, the CCSD(T)/aD and CCSD(T)/aT values differ by up to 0.4 kcal/mol. On the basis of the above observations for the dimer, the CCSD(T)/aT values should be very close to the CCSD(T)/CBS values. Similarly, the core−valence corrections are likely to be slightly smaller than the calculated values at the CCSD(T)/awCVDZ level, which range from 3.7 to 5.0 kcal/mol. The calculated scalar relativistic corrections for the trimer and tetramer are 0.4−0.5 kcal/mol, slightly larger than those for the dimer. The ZPE corrections for the trimer and tetramer are 1.3−1.5 kcal/mol, again slightly larger than those for the dimer. For the differential clustering energy, the CCSD(T)/aT value is nearly identical to the CCSD(T)/aD value for the (C_s **a**) structure of the trimer and is ∼0.6 kcal/mol larger than that for the C_2 structure. For the tetramer, the CCSD(T)/aT values are larger than the CCSD(T)/aD values for the (C_{2v} **a**) and (C_{2v} **b**) structures by ∼0.8 and 1.2 kcal/mol, respectively, and the CCSD(T)/aT value is smaller than the CCSD(T)/aD value by ∼0.5 kcal/mol for the (C_{2h} **a**) structure. The core−valence corrections calculated at the CCSD(T)/awCVDZ level range from 6.1 to 6.4 kcal/mol for the trimer, 7.7 to 8.3 kcal/mol for the (C_{2v} **a**) and (C_{2h} **a**) structures of the tetramer, and ∼4.3 kcal/mol for the (C_{2v} **b**) structure of the tetramer. The scalar relativistic and ZPE corrections are significantly smaller, ranging from 0.7 to 0.9 and 1.4 to 1.9 kcal/mol for the trimer and tetramer, respectively.

We have previously calculated the dimerization energy (negative of the differential clustering energy) for M_2O_6 (M = Cr, Mo, W) at 0 K as −93.6, −113.3, and −128.7 kcal/mol at

TABLE 9: Normalized and Differential Clustering Energies at 0 K (ΔE_{0K}, kcal/mol) for $(TiO_2)_n$ ($n = 2-4$) Calculated at the CCSD(T), B3LYP/aT//B3LYP/aD, BP86/aT//BP86/aD, and PW91/aT//PW91/aD Levels

		CCSD(T) [a,b]	B3LYP[b]	BP86	PW91
		Normalized			
Ti_2O_4	^1A_g (C_{2h})	61.2	57.8	55.2	56.2
Ti_3O_6	$^1A'$ (C_s **a**)	85.0	77.2	73.2	74.8
Ti_4O_8	$^1A_1$ (C_{2v} **a**)	98.4	88.2	83.4	85.3
		Differential			
Ti_2O_4	^1A_g (C_{2h})	122.5	115.6	110.4	112.4
Ti_3O_6	$^1A'$ (C_s **a**)	131.1	116.1	109.2	111.9
Ti_4O_8	$^1A_1$ (C_{2v} **a**)	138.3	121.1	114.2	116.9

[a] CCSD(T)/CBS for $n = 1$ and 2, CCSD(T)/aT for $n = 3$ and 4. [b] ZPEs from BP86/aD.

the CCSD(T)/CBS level.[38] Thus the differential clustering energy for the most stable conformer of Ti_2O_4 of 122.5 kcal/mol is ~29 and 9 kcal/mol larger than those of Cr_2O_6 and Mo_2O_6, respectively, and ~6 kcal/mol smaller than that of W_2O_6. We note that the structural changes are similar as a terminal μ-oxo M=O bond on each monomer is converted to a bridge M−O−M bond in the dimer for TiO_2 and for MO_3.

Table 9 shows the normalized and differential clustering energies calculated at the B3LYP/aT//B3LYP/aD, BP86/aT//BP86/aD, and PW91/aT//PW91/aD levels as compared to those calculated at the CCSD(T) level. For the normalized clustering energy, the B3LYP/aT//B3LYP/aD values are smaller than the CCSD(T) values, by ~3 kcal/mol for the dimer, ~8 kcal/mol for the trimer, and ~10 kcal/mol for the tetramer. The BP86/aT//BP86/aD values are slightly smaller than the PW91/aT//PW91/aD values by 1−2 kcal/mol, and the PW91/aT//PW91/aD values are smaller than the CCSD(T) values by ~5 kcal/mol for the dimer, ~10 kcal/mol for the trimer, and ~13 kcal/mol for the tetramer. Similar conclusions can be drawn for the differential clustering energy, with larger differences between the DFT and CCSD(T) values.

Previous studies on the group VIB transition metal oxide clusters have shown that the normalized clustering energies are nearly converged at $n = 3$, although they continue to increase for larger n.[38] For these clusters, the differential clustering energies decrease as n increases from 2 to 5.[38] This behavior is very different from the titanium dioxide clusters, where the normalized clustering energies are not converged at $n = 4$ and the differential clustering energies increase as n increases from 2 to 4.

3.10. Heats of Formation. Table 10 shows the calculated atomization energies at 0 K at the CCSD(T) level for the $(TiO_2)_n$ ($n = 1-4$) clusters. Different contributions to the atomization energies are shown to assess the relative importance of the different corrections. The atomization energies at 0 K for the monomer and dimer have been estimated to be 301 ± 3 and 721 ± 11 kcal/mol by high pressure mass spectroscopy and these error bars could be larger.[20,21] At the CCSD(T)/CBS level, the atomization energies of the monomer and the most stable conformer of the dimer are calculated to be 297.9 and 718.4 kcal/mol, in excellent agreement with the estimated experimental values, especially considering the large error bars in the experimentally estimated values.

For the monomer and dimer, the CBS extrapolation contributions to the atomization energies from the aD basis set are ~19 kcal/mol for the monomer, and ~40 kcal/mol for the dimer. Those from the aT basis set are 8.2 kcal/mol for the monomer, and 16.8 kcal/mol for the dimer. Thus, the basis set size effect is much more substantial for the atomization energies than for the relative energies, electron detachment energies, and clustering energies. This is not surprising as the atomization energy is the energy required to dissociate the cluster into atoms, and large basis sets in the correlation treatment are necessary to account for the dramatic change of the chemical environment from the cluster to the atoms. The CBS extrapolation contribution for the dimer is about twice as large as that for the monomer. Thus, we can estimate the CBS extrapolation contributions from aT to CBS for the atomization energies for the trimer and tetramer from those for the monomer and dimer to be 25.1 and 33.3 kcal/mol, respectively. These estimates are included in Table 10 to reduce the errors in the calculated atomization energies for the trimer and tetramer.

Another means to estimate the total atomization energy for the larger clusters is to use a group additivity approach, where we consider the TiO_2 to be the group. As noted above, the normalized clustering energies $\Delta E_{norm,n}$ are not strongly dependent on the basis set. Thus we can use eq 7 to estimate the atomization energy of a cluster:

$$\sum D_{0,0K}[(TiO_2)_n] = n \sum D_{0,0K}(TiO_2) + n\Delta E_{norm,n} \quad (7)$$

For the trimer and tetramer, the atomization energies estimated from eq 7 from the CCSD(T)/CBS atomization energy of the monomer and the CCSD(T)/aT normalized clustering energies of the trimer and tetramer are 1148.9 and 1585.2 kcal/mol, respectively. These are in excellent agreement with the estimated values of 1145.3 and 1580.2 kcal/mol for the trimer and tetramer using the approach in the previous paragraph.

For the core−valence correction to the atomization energy, the CCSD(T)/awCVTZ value is ~1.3 kcal/mol larger than that at the CCSD(T)/awCVDZ level for the monomer and 0.7−0.8 kcal/mol larger for the C_{2h} and (C_{2v} **a**) structures of the dimer, but it is ~0.1 kcal/mol smaller for the C_{3v} structure of the dimer. Thus, it is difficult to estimate accurately the error induced by calculating the core−valence corrections at the CCSD(T)/awCVDZ level for the trimer and tetramer. The scalar relativistic correction to the atomization energy is ~0.8 kcal/mol for the monomer and ~2.2 kcal/mol for the dimer. The ZPE corrections are ~3.3 kcal/mol for the monomer and 8.2−8.7 kcal/mol for the dimer.

Table 11 presents the calculated heats of formation at 0 and 298 K for the $(TiO_2)_n$ ($n = 1-4$) clusters. The heats of formation are calculated from the CCSD(T) atomization energies shown in Table 10 and the B3LYP, BP86, and PW91 atomization energies given in the Supporting Information. For the trimer and tetramer, the heats of formation can be calculated with three different approaches: (1) with the CCSD(T) atomization energies corrected by the estimated aT to CBS extrapolation effects; (2) from the CCSD(T)/CBS heats of formation of the monomer and the normalized CCSD(T)/aT clustering energies of the trimer and tetramer (eq 8); and (3) by building up from the $n - 1$ cluster by using the CCSD(T)/CBS heats of formation of the monomer, the differential clustering energy (eq 8), and the heat of formation of the $n - 1$ cluster.

$$\Delta H_{f,0K}(Ti_nO_{2n}) = n\Delta H_{f,0K}(TiO_2) - n\Delta E_{norm,n}(Ti_nO_{2n}) \quad (8)$$

$$\Delta H_{f,0K}(Ti_nO_{2n}) = \Delta H_{f,0K}(TiO_2) + \Delta H_{f,0K}(Ti_{n-1}O_{2(n-1)}) - \Delta E_{diff,n}(Ti_nO_{2n}) \quad (9)$$

Results from these three approaches agree within a few kcal/mol. The "experimental" heats of formation of the monomer and dimer are calculated from the experimentally estimated atomization energies[20,21] and the experimental heats of formation for the atoms,[98,99] which yields heats of formation of −71 ± 4 and −260 ± 12 kcal/mol at 0 K for the monomer and dimer,

TABLE 10: Atomization Energies at 0 K ($\Sigma D_{0,0K}$, kcal/mol) for $(TiO_2)_n$ ($n = 1-4$) Calculated at the CCSD(T) Level and Compared with Available Experimental Data

		ΔE_{aD}[a]	ΔE_{aT}[b]	ΔE_{aQ}[b]	ΔE_{CBS}[c]	$\Delta E_{CV(D)}$[b,d]	$\Delta E_{CV(T)}$[b,e]	ΔE_{SR}[b,f]	ΔE_{ZPE}[g]	ΔE_{SO}[h]	$\Sigma D_{0,0K}$[i]	expt[j]
TiO_2	$^1A_1$ (C_{2v})	280.73	291.55	296.67	299.77	+1.96	+3.30	−0.78	−3.26	−1.08	297.9	301 ± 3
Ti_2O_4	^1A_g (C_{2h})	682.83	704.79	715.26	721.59	+9.01	+9.80	−2.19	−8.67	−2.16	718.4	721 ± 11
Ti_3O_6	$^1A'$ (C_s **a**)	1090.72	1123.48			+17.42		−3.62	−13.78	−3.25	1145.3[k,l]	
Ti_4O_8	$^1A_1$ (C_{2v} **a**)	1504.08	1548.46			+27.03		−5.27	−18.95	−4.33	1580.2[k,l]	

[a] Geometries from CCSD(T)/aD for $n = 1$ and 2, and from B3LYP/aD for $n = 3$ and 4. [b] Geometries from CCSD(T)/aT for $n = 1$ and 2, and from B3LYP/aD for $n = 3$ and 4. [c] Extrapolated using the mixed Gaussian/exponential formula for the CCSD(T) energies with the aD, aT, and aQ basis sets. [d] CCSD(T)/awCVDZ. [e] CCSD(T)/awCVTZ. [f] CISD/aT. [g] BP86/aD. [h] The spin−orbit corrections for the atoms are calculated as $\{\sum_J(2J+1)\cdot E_J\}/\{\sum_J(2J+1)\}$. [i] $D_{0,0K} = \Delta E_{CBS} + \Delta E_{CV(T)} + \Delta E_{SR} + \Delta E_{ZPE} + \Delta E_{SO}$ for $n = 1$ and 2, $\Delta E_{aT} + \Delta E_{CV(D)} + \Delta E_{SR} + \Delta E_{ZPE} + \Delta E_{SO}$ for $n = 3$ and 4. [j] References 20 and 21. [k] Estimates for the extrapolation effects from aT to CBS are included. The extrapolation from aT to CBS is estimated to be 25.1 kcal/mol for $n = 3$ and 33.3 kcal/mol for $n = 4$. [l] The atomization energies of the trimer and tetramer is estimated to be 1148.9 and 1585.2 kcal/mol, respectively, from the CCSD(T)/CBS atomization energy of the monomer and the CCSD(T)/aT normalized clustering energies of the trimer and tetramer.

TABLE 11: Heats of Formation at 0 and 298 K ($\Delta H_{f,0K}$ and $\Delta H_{f,298K}$, kcal/mol) Calculated with the CCSD(T), B3LYP, BP86, and PW91 Methods,[a] and Compared with the Experimental Values

		CCSD(T)[b]		B3LYP[c]		BP86[c]		PW91[c]		
molecule		$\Delta H_{f,0K}$[e]	$\Delta H_{f,298K}$[f]	$\Delta H_{f,0K}$[e]	$\Delta H_{f,298K}$[f]	$\Delta H_{f,0K}$[e]	$\Delta H_{f,298K}$[f]	$\Delta H_{f,0K}$[e]	$\Delta H_{f,298K}$[f]	expt[d] $\Delta H_{f,0K}$
TiO_2	$^1A_1$ (C_{2v})	−67.6	−68.2	−58.1	−58.7	−104.7	−105.2	−107.9	−108.5	−71 ± 4
Ti_2O_4	^1A_g (C_{2h})	−257.6	−259.4	−231.8	−233.6	−319.7	−321.5	−328.2	−329.9	−260 ± 12
Ti_3O_6	$^1A'$ (C_s **a**)	−454.3, −457.8[g], −456.3[h]	−457.1, −460.6[g], −459.1[h]	−406.2	−409.1	−533.6	−536.4	−547.9	−550.8	
Ti_4O_8	$^1A_1$ (C_{2v} **a**)	−658.8, −662.0[g], −660.2[h]	−662.9, −668.1[g], −664.3[h]	−585.6	−589.6	−752.5	−756.5	−772.7	−776.8	

[a] Error bars due to errors in the heats of formation of the atoms are ±0.7 for TiO_2, ±1.4 for Ti_2O_4, ±2.1 for Ti_3O_6, ±2.8 for Ti_4O_8. [b] Using the atomization energies shown in Table 1. [c] Using the atomization energies calculated at the B3LYP/aT//B3LYP/aD, BP86/aT//BP86/aD, and PW91/aT//PW91/aD levels given in the Supporting Information. [d] Derived from the estimated atomization energies from refs 20 and 21, and the experimental heats of formation for the atoms from refs 98 and 99. [e] $\Delta H_{f,0K}(Ti_nO_{2n}) = n\Delta H_{f,0K}(Ti) + 2n\Delta H_{f,0K}(O) - \Sigma D_{0,0K}(Ti_nO_{2n})$, where the experimental $\Delta H_{f,0K}$ (58.98 ± 0.02, 112.4 ± 0.7 kcal/mol for O and Ti) were used for the atoms. [f] $\Delta H_{f,298K}(Ti_nO_{2n}) = \Delta H_{f,0K}(Ti_nO_{2n}) + \Delta H_{0K\rightarrow 298K}(Ti_nO_{2n}) - n\Delta H_{0K\rightarrow 298K}(Ti) - 2n\Delta H_{0K\rightarrow 298K}(O)$. The experimental enthalpy change from 0 to 298 K ($\Delta H_{0K\rightarrow 298K}$) is 1.04 and 1.15 kcal/mol for O and Ti, respectively. The enthalpy change from 0 to 298 K for Ti_nO_{2n} calculated at the BP86/aD level is used. [g] $\Delta H_{f,0K}(Ti_nO_{2n}) = n\Delta H_{f,0K}(TiO_2) - n\Delta E_{norm,n}(Ti_nO_{2n})$. [h] $\Delta H_{f,0K}(Ti_nO_{2n}) = \Delta H_{f,0K}(TiO_2) + \Delta H_{f,0K}(Ti_{n-1}O_{2(n-1)}) - \Delta E_{diff,n}(Ti_nO_{2n})$.

respectively. The large error bars in the experimental heats of formation arise from the large uncertainty in the experimentally estimated atomization energies of the clusters.[20,21] The heats of formation at 0 K of the monomer and dimer are calculated at the CCSD(T)/CBS level to be −67.6 ± 0.7 and −257.6 ± 1.4 kcal/mol, respectively, where the error bars are due to errors in the atomic heats of formation, They are in good agreement with the experimental values, consistent with the good agreement for the total atomization energies.

The calculated heats of formation at the B3LYP/aT//B3LYP/aD level are ∼10 and 26 kcal/mol less negative than the CCSD(T)/CBS values for the monomer and dimer, respectively. The BP86/aT//BP86/aD and PW91/aT//PW91/aD heats of formation, on the other hand, are ∼40 and ∼65 kcal/mol more negative than the CCSD(T)/CBS values for the monomer and dimer, respectively. The large differences in the calculated heats of formation at the B3LYP level, and especially at the BP86 and PW91 levels for the titanium dioxide clusters follow the trends found for the heats of formation of group VIB transition metal oxide clusters.[38] These large differences cannot be attributed to the incompleteness of the basis set we used for the DFT calculations, as the atomization energy calculated at the B3LYP/aQ//B3LYP/aD level differ from the B3LYP/aD value by <0.5 kcal/mol for the monomer. The poor performance of the BP86 and PW91 functionals in the calculated heats of formation for these oxide clusters may be related to their inability to predict accurate values for the dissociation energy of O_2.[38] The experimental dissociation energy is 118.0 kcal/mol.[104] The calculated dissociation energy is 139.1 and 140.3 kcal/mol at the BP86/aT//B3LYP/aD and PW91/aT//B3LYP/aD levels, respectively, and 120.8 and 118.1 kcal/mol at the B3LYP/aT//B3LYP/aD and CCSD(T)/CBS levels.[38] The BP86 and PW91 functionals predict O_2 to be overbound. The DFT normalized clustering energies are enough in error that we cannot really use them with the accurate value for the atomization energy of TiO_2 to predict accurate atomization energies and heats of formation using eqs 7–9. We note that if a functional can be found that provides better estimates of the clustering energies, then we can apply eqs 7–9 to obtain reliable atomization energies and heats of formation of much larger clusters.

3.11. Bond Energies. The average Ti=O μ-oxo bond dissociation energy (BDE) at 0 K obtained from the atomization energy for TiO_2 is 149.0 kcal/mol at the CCSD(T)/CBS level. The average M=O μ-oxo BDEs for MO_3 (M = Cr, Mo, W) have been estimated to be 111.2, 137.6, and 153.4 kcal/mol for M = Cr, Mo, and W, respectively, at the same level of theory.[38] Thus these metal μ-oxo average BDEs are quite large and increase in the order of Cr < Mo < Ti < W. We note that the average Ti=O μ-oxo BDE is predicted to be only slightly smaller than the W=O μ-oxo bond energy. The metal μ-oxo bonds are expected to be strong due to the ionic nature of the interactions and the backbonding between the filled O pπ orbitals and the empty M dπ orbitals.[38]

If we assume that the Ti=O bond energy in TiO_2 is the same as that in Ti_2O_4 (C_{2h}), then we can estimate the average BDE of the Ti−O bridge bonds in Ti_2O_4 as follows: $E(Ti-O) = {}^1/_4\Sigma D_{0,0K}(Ti_2O_4) - 2E(Ti=O)]$. This gives $E(Ti-O) = 105.1$ kcal/mol at the CCSD(T)/CBS level, which can be compared to the values of 78.0, 97.1, and 108.8 kcal/mol for the Cr−O, Mo−O, and W−O, respectively, calculated with a similar formula.[38] The M−O BDEs follow the same order as that for

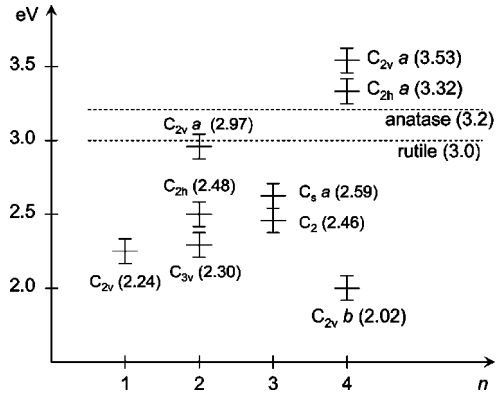

Figure 8. Adiabatic energy gaps for the low-lying structures of the $(TiO_2)_n$ ($n = 1-4$) clusters calculated at the CCSD(T)/aD//B3LYP/aD level relative to those of the bulk values from ref 105.

the M═O BDEs. The above arguments about the average BDEs of the M═O bonds also apply to those of the M−O bonds.

Similarly, we can estimate the BDE of the triple-bridge titanium−oxygen bond in the (C_s **a**) structure of the trimer as $\Sigma D_{0,0K}(Ti_3O_6) - 2E(Ti{=}O) - 6E(Ti-O) = 216.7$ kcal/mol. It is larger than twice the average Ti−O BDE by ∼7 kcal/mol. Without the triple-bridge titanium−oxygen bond, the C_2 structure of the trimer is ∼15 kcal/mol higher in energy, which is reasonably close to the energy difference estimated from the titanium−oxygen BDEs of ∼7 kcal/mol. For the (C_{2v} **a**) structure of the tetramer, the quadruple-bridge titanium−oxygen BDE can be estimated as $\Sigma D_{0,0K}(Ti_4O_8) - 2E(Ti{=}O) - 10E(Ti-O) = 231.2$ kcal/mol. It is greater than twice the average Ti−O BDE by ∼21 kcal/mol, modestly stronger than the triple-bridge titanium−oxygen bond. With two triple-bridge titanium−oxygen bonds, the (C_{2h} **a**) is only ∼5 kcal/mol higher in energy than the (C_{2v} **a**) structure, which is close to the energy difference estimated from the titanium−oxygen BDEs of ∼7 kcal/mol. With no triple- or quadruple-bridge titanium−oxygen bonds, the (C_{2v} **b**) structure is ∼16 kcal/mol higher in energy, which is consistent with the estimated energy difference of ∼21 kcal/mol based on the titanium−oxygen BDEs.

3.12. Catalytic Implications. TiO_2 with band gaps of 3.0 eV for rutile and 3.2 eV for anatase,[105] is an active photocatalyst. As shown in Table 6, the experimental energy gaps have been measured to be ∼2.2 eV for the monomer and trimer, and ∼2.6 eV for the dimer and tetramer.[26] Furthermore, our CCSD(T) and DFT calculations show that the energy gaps exhibit a strong dependence on the cluster structures. Figure 8 displays the adiabatic energy gaps (the energy differences between the first triplet excited states and the ground states of the neutral clusters) at the CCSD(T)/aD//B3LYP/aD level. The first singlet and triplet excited states of these clusters are energetically nearly degenerate so these adiabatic energy gaps are good approximations to the first singlet excitation energies for the clusters. The calculated adiabatic energy gaps are ∼2.2 eV for the monomer, 2.3−3.0 eV for the low-lying structures of the dimer, 2.4−2.6 eV for the trimer, and 2.1−3.5 eV for the tetramer. These gaps, except for the tetramer are below the band gap of the bulk material and show that controlling the particle size and structure will be important in controlling the photocatalytic activity of TiO_2 nanoparticles. The energies of the ground state of the low-lying conformations lie within ∼15 kcal/mol at the CCSD(T) level to the ground states of these clusters. Thus, they may be present on the surface of TiO_2 catalysts, depending on the manufacturing process, the support, and other environmental effects. This could be one of the reasons for the strong dependence of the photocatalytic activity of titanium dioxide particles on the manufacturing process. As there are a number of low-lying structures with distinct energy gaps, one should be able to change the photocatalytic properties of the titanium dioxide particles by varying the size and structural distribution with different preparation methods and/or different supports. In fact, recent studies on the photocatalytic reduction of NO using the Ti-MCM-41 catalyst revealed that tetrahedrally coordinated Ti oxide species are the active sites, and that the catalytic activity is shown to strongly dependent on the local structure of the Ti oxide species.[5] An important feature is that the band gap of the cluster can be tuned to be more in the visible region so that the TiO_2 particles can more efficiently absorb solar radiation at the Earth's surface.

The anions of these small clusters can have different structures with which are very close in energy for the dimer and tetramer. Furthermore, the extra electron is localized on a single metal center for the monomer and trimer but is partially delocalized on two Ti centers for the dimer and tetramer. In most cases, the extra electron in the anion is localized in the Ti $3d_{z^2}$ orbitals except for the monomer and the (C_{2v} **a**) and (C_{2h} **a**) structures of the tetramer where other d orbitals are involved. All these anions contain electron-rich titanium center(s) with strong electron donating capability. These anions are expected to be very reactive, which may contribute to the photocatalytic activity of titanium dioxide.

4. Conclusions

Coupled cluster [CCSD(T)] theory and density functional theory (DFT) have been used to study the structural and energetic properties of the $(TiO_2)_n$ ($n = 1-4$) clusters and their anions. Electron detachment energies of the low-lying conformations of the anions and the first excitation energies of the corresponding neutral clusters have been calculated and compared with the photoelectron spectral data. The ground-state structures of the anions are determined on the basis of such comparison. The ground-state structures predicted by the DFT method with the B3LYP, BP86, and PW91 functionals are the same as those from the CCSD(T) method except for the anions of the dimer and tetramer. For the calculations of relative energies and electron detachment energies, a relatively small basis set extrapolation effect is found for these clusters, which enables the accurate calculations of these energetics with the triplet zeta basis set at the CCSD(T) level for the trimer and tetramer. In addition, the core−valence and zero-point corrections are found to be more important than the scalar relativistic corrections in calculating these properties. The calculated first excitation energies are shown to strongly depend on the size as well as the structure of the cluster.

Normalized and differential clustering energies, atomization energies, and heats of formation for the neutral clusters have been calculated and compared with available experimental data. For the clustering energies, the basis set extrapolation and scalar relativistic contributions are found to be much smaller than the core−valence and zero-point corrections, but for the atomization energies, these terms can be quite substantial. However, the atomization energies for the larger clusters can be significantly improved by estimating the CBS extrapolation effects from the smaller clusters. The calculated heats of formation can also be vastly improved by using the calculated clustering energies and the calculated heats of formation for the smaller clusters. This provides a general method for calculating accurate heats of formation for relatively large transition metal oxide clusters. The normalized clustering energies are not converged at $n = 4$,

in contrast to the case for the group VIB transition metal oxide clusters where convergence is achieved at $n = 3$.[96] The calculated M=O and M−O bond energies for M = Ti are found to be larger than those for M = Cr and Mo, but slightly smaller than those for M = W.

Acknowledgment. This work was supported by the Chemical Sciences, Geosciences and Biosciences Division, Office of Basic Energy Sciences, U.S. Department of Energy (DOE) under grant no. DE-FG02-03ER15481 (catalysis center program) and by the National Science Foundation (CTS-0608896), through the NIRT program. D.A.D. also thanks the Robert Ramsay Chair Fund of The University of Alabama for support. Part of this work was performed at the W. R. Wiley Environmental Molecular Sciences Laboratory, a national scientific user facility sponsored by DOE's Office of Biological and Environmental Research and located at Pacific Northwest National Laboratory, operated for the DOE by Battelle.

Supporting Information Available: Geometry parameters at different computational levels, relative energies for different structures of a given cluster at 0 K at the B3LYP/aD, BP86/aD, PW91/aD levels and at 298 K at the CCSD(T) level, electron detachment energies to the ground state and first triplet excited states of the neutral clusters at the B3LYP/aD, BP86/aD, PW91/aD levels, reorganization energies and adiabatic energy gaps at the B3LYP/aD, BP86/aD, PW91/aD levels, clustering energies at 0 K at the B3LYP/aD, BP86/aD, and PW91/aD levels and at 298 K at the CCSD(T) level, DFT atomization energies, heats of formation at 0 and 298 K at the B3LYP/aD, BP86/aD, and PW91/aD levels, zero-point energies and electronic energies (E_e) at different computational levels calculated at the B3LYP/aD, BP86/aD, PW91/aD, CCSD(T)/aD, and CCSD(T)/aT optimized geometries, CCSD T_1 diagnostics, and Cartesian coordinates in Angstroms optimized at the B3LYP/aD, BP86/aD, PW91/aD, CCSD(T)/aD, and CCSD(T)/aT levels. Figure S1 showing structures of the rutile (a) and anatase (b) phases of bulk TiO_2 and Figure S2 showing additional high energy structures of $(TiO_2)_n^-$ ($n = 2-4$). This material is available free of charge via the Internet at http://pubs.acs.org.

References and Notes

(1) Greenwood,N. N. ; Earnshaw,A. *Chemistry of the Elements*, 2nd ed.; Pergamon Press: Oxford, U.K., 1984.
(2) Cotton, F. A. ; Wilkinson, G. ; Murillo, C. A. ; Bochmann, M. *Advanced Inorganic Chemistry*, 6th ed.; Wiley: New York, 1999.
(3) Wachs, I. E. In *Metal Oxides: Chemistry and Applications*; Fierro, J. L. G., Ed.;CRC Press: Boca Raton, FL, 2006; pp 1−30.
(4) Thompson, T. L.; Yates, J. T. *Chem. Rev.* **2006**, *106*, 4428.
(5) Anpo, M.; Dohshi, S.; Kitano, M. ; Hu, Y. In *Metal Oxides: Chemistry and Applications*; Fierro, J. L. G., Ed.; CRC Press: Boca Raton, FL, 2006; pp 622.
(6) Grätzel, M. *Nature* **2001**, *414*, 338.
(7) Fujishima, A.; Hashimoto, K.; Watanabe, H. TiO_2 *Photocatalysis: Fundamentals and Applications*; BKC, Inc.: Tokyo,1997.
(8) Meagher, E. P.; Larger, G. A. *Can. Mineral.* **1979**, *17*, 77.
(9) Gonschorek, W.; Feld, R. *Z. Kristallogr.* **1982**, *136*, 273.
(10) Gonschorek, W. *Z. Kristallogr.* **1982**, *161*, 1.
(11) Restori, R.; Schwarzenbach, D.; Schneider, J. R. *Acta Crystallogr.* **1987**, *43*, 251.
(12) Sugiyama, K.; Takeuchi, Y. *Z. Kristallogr.* **1991**, *194*, 305.
(13) Horn, M.; Schwerdtfeger, C. F.; Meagher, E. P. *Z. Kristallogr.* **1972**, *136*, 273.
(14) Gribb, A. A.; Banfield, J. F. *Am. Mineral.* **1997**, *82*, 717.
(15) Zhang, H.; Banfield, J. F. *J. Mater. Chem.* **1998**, *8*, 2073.
(16) Muscat, J.; Swamy, V.; Harrison, N. M. *Phys. Rev. B* **2002**, *65*, 224112.
(17) Kaufman, M.; Muenter, J.; Klemperer, W. *J. Chem. Phys.* **1967**, *47*, 3365.
(18) McIntyre, N. S.; Thompson, K. R.; Weltner, W., Jr. *J. Phys. Chem.* **1971**, *75*, 3243.
(19) Chertihin, G. V.; Andrews, L. *J. Phys. Chem.* **1995**, *99*, 6356.
(20) Balducci, G.; Gigli, G.; Guido, M. *J. Chem. Phys.* **1985**, *83*, 1909.
(21) Balducci, G.; Gigli, G.; Guido, M. *J. Chem. Phys.* **1985**, *83*, 1913.
(22) Koyanagi, G. K.; Caraiman, D.; Blagojevic, V.; Bohme, D. K. *J. Phys. Chem. A* **2002**, *106*, 4581.
(23) Yu, W.; Freas, R. B. *J. Am. Chem. Soc.* **1990**, *112*, 7126.
(24) Guo, B. C.; Kerns, K. P.; Castleman, A. W., Jr *Int. J. Mass Spectrom. Ion Processes* **1992**, *117*, 129.
(25) Wu, H.; Wang, L.-S. *J. Chem. Phys.* **1997**, *107*, 8221.
(26) Zhai, H.-J.; Wang, L.-S. *J. Am. Chem. Soc.* **2007**, *129*, 3022.
(27) Foltin, M.; Stueber, G. J.; Bernstein, E. R. *J. Chem. Phys.* **1999**, *111*, 9577.
(28) Matsuda, Y.; Bernstein, E. R. *J. Phys. Chem. A* **2005**, *109*, 314.
(29) Von Helden, G.; van Heijnsbergen, D.; Meijer, G. *J. Phys. Chem. A* **2003**, *107*, 1671.
(30) Demyk, K.; van Heijnsbergen, D.; von Helden, G.; Meijer, G. *Astr. Astrophys.* **2004**, *420*, 547.
(31) Parr, R. G.; Yang, W. *Density-Functional Theory of Atoms and Molecules*; Oxford University Press: New York, 1989.
(32) Ramana, M. V.; Phillips, D. H. *J. Chem. Phys.* **1988**, *88*, 2637.
(33) Bergstrom, R.; Lunell, S.; Eriksson, L. A. *Int. J. Quantum Chem.* **1996**, *59*, 427.
(34) Becke, A. D. *Phys. Rev. A* **1988**, *38*, 3098.
(35) Lee, C.; Yang, W.; Parr, R. G. *Phys. Rev. B* **1988**, *37*, 785.
(36) Perdew, J. P. *Phys. Rev. B* **1986**, *33*, 8822.
(37) Becke, A. D. *J. Chem. Phys.* **1993**, *98*, 5648.
(38) Li, S.; Dixon, D. A. *J. Phys. Chem.* **2007**, *111*, 11908.
(39) Purvis, G. D., III; Bartlett, R. J. *J. Chem. Phys.* **1982**, *76*, 1910.
(40) Raghavachari, K.; Trucks, G. W.; Pople, J. A.; Head-Gordon, M. *Chem. Phys. Lett.* **1989**, *157*, 479.
(41) Watts, J. D.; Gauss, J.; Bartlett, R. J. *J. Chem. Phys.* **1993**, *98*, 8718.
(42) Bartlett, R. J.; Musial, M. *Rev. Mod. Phys.* **2007**, *79*, 291.
(43) Walsh, M. B.; King, R. A.; Schaefer, H. F., III *J. Chem. Phys.* **1999**, *110*, 5224.
(44) Gutsev, G. L.; Rao, B. K.; Jena, P. *J. Phys. Chem. A* **2000**, *104*, 11961.
(45) Grein, F. *J. Chem. Phys.* **2007**, *126*, 34313.
(46) Hagfeldt, A.; Bergstrom, R.; Siegbahn, H. O. G.; Lunell, S. *J. Phys. Chem.* **1993**, *97*, 12725.
(47) Albaret, T.; Finocchi, F.; Noguera, C. *J. Chem. Phys.* **2000**, *113*, 2238.
(48) Jeong, K. S.; Chang, C.; Sedlmayr, E.; Sulzle, D. *J. Phys. B* **2000**, *33*, 3417.
(49) Hamad, S.; Catlow, C. R. A.; Woodley, S. M.; Lago, S.; Mejias, J. A. *J. Phys. Chem. B* **2005**, *109*, 15741.
(50) Qu, Z.-W.; Kroes, G.-J. *J. Phys. Chem. B* **2006**, *110*, 8998.
(51) Burke, K. ; Perdew, J. P. Wang, Y. In *Electronic Density Functional Theory: Recent Progress and New Directions*; Dobson, J. F.,Vignale, G., Das, M. P., Eds.; Plenum: New York, 1998.
(52) Perdew, J. P.; Wang, Y. *Phys. Rev. B* **1991**, *45*, 13244.
(53) Kendall, R. A.; Dunning, T. H., Jr.; Harrison, R. J. *J. Chem. Phys.* **1994**, *96*, 6796.
(54) Peterson, K. A.; Figgen, D.; Dolg, M.; Stoll, H. *J. Chem. Phys.* **2007**, *126*, 124101. Peterson, K.A. Unpublished basis sets for the first and third row transition metals.
(55) Peterson, K. A.; Woon, D. E.; Dunning, T. H., Jr *J. Chem. Phys.* **1994**, *100*, 7410.
(56) Woon, D. E.; Dunning, T. H., Jr *J. Chem. Phys.* **1995**, *103*, 4572.
(57) Peterson, K. A.; Dunning, T. H., Jr *J. Chem. Phys.* **2002**, *117*, 10548.
(58) Feller, D.; Peterson, K. A. *J. Chem. Phys.* **1998**, *108*, 154.
(59) Dixon, D. A.; Feller, D. *J. Phys. Chem. A* **1998**, *102*, 8209.
(60) Feller, D.; Peterson, K. A. *J. Chem. Phys.* **1999**, *110*, 8384.
(61) Feller, D.; Dixon, D. A. *J. Phys. Chem. A* **1999**, *103*, 6413.
(62) Feller, D. *J. Chem. Phys.* **1999**, *111*, 4373.
(63) Feller, D.; Dixon, D. A. *J. Phys. Chem. A* **2000**, *104*, 3048.
(64) Feller, D.; Sordo, J. A. *J. Chem. Phys.* **2000**, *113*, 485.
(65) Feller, D.; Dixon, D. A. *J. Chem. Phys.* **2001**, *115*, 3484.
(66) Ruscic, B.; Wagner, A. F.; Harding, L. B.; Asher, R. L.; Feller, D.; Dixon, D. A.; Peterson, K. A.; Song, Y.; Qian, X.; Ng, C.; Liu, J.; Chen, W.; Schwenke, D. W. *J. Phys. Chem. A* **2002**, *106*, 2727.
(67) Feller, D.; Dixon, D. A.; Peterson, K. A. *J. Phys. Chem. A* **1998**, *102*, 7053.
(68) Dixon, D. A.; Feller, D; Peterson, K. A. *J. Chem. Phys.* **2001**, *115*, 2576.
(69) Dixon, D. A.; Gutowski, M. *J. Phys. Chem. A* **2005**, *109*, 5129.
(70) Grant, D.; Dixon, D. A. *J. Phys. Chem. A* **2005**, *109*, 10138.
(71) Matus, M. H.; Anderson, K. D.; Camaioni, D. M.; Autrey, S. T.; Dixon, D. A. *J. Phys. Chem. A* **2007**, *111*, 4411.
(72) Pollack, L.; Windus, T. L.; de Jong, W. A.; Dixon, D. A. *J. Phys. Chem. A* **2005**, *109*, 6934.

(73) Jamorski, C.; Casida, M. E.; Salahub, D. R. *J. Chem. Phys.* **1996**, *104*, 5134.

(74) Bauernschmitt, R.; Ahlrichs, R. *Chem. Phys. Lett.* **1996**, *256*, 454.

(75) Bauernschmitt, R.; Häser, M.; Treutler, O.; Ahlrichs, R. *Chem. Phys. Lett.* **1997**, *264*, 573.

(76) Hirata, S.; Head-Gordon, M. *Chem. Phys. Lett.* **1999**, *314*, 291.

(77) Casida, M. E.; Salahub, D. R. *J. Chem. Phys.* **2000**, *113*, 8918.

(78) Hirata, S.; Zhan, C.-G.; Aprà, E.; Windus, T. L.; Dixon, D. A. *J. Phys. Chem. A* **2003**, *107*, 10154.

(79) Zhan, C.-G.; Nicholas, J. A.; Dixon, D. A. *J. Phys. Chem. A* **2003**, *107*, 4184.

(80) Zhai, H.-J.; Li, S.; Dixon, D. A.; Wang, L.-S. *J. Am. Chem. Soc.* **2008**, *112*, 4095.

(81) Frisch, M. J.; Trucks, G. W.; Schlegel, H. B.; Scuseria, G. E.; Robb, M. A.; Cheeseman, J. R.; Montgomery, J. A., Jr.; Vreven, T.; Kudin, K. N.; Burant, J. C.; Millam, J. M.; Iyengar, S. S.; Tomasi, J.; Barone, V.; Mennucci, B.; Cossi, M.; Scalmani, G.; Rega, N.; Petersson, G. A.; Nakatsuji, H.; Hada, M.; Ehara, M.; Toyota, K.; Fukuda, R.; Hasegawa, J.; Ishida, M.; Nakajima, T.; Honda, Y.; Kitao, O.; Nakai, H.; Klene, M.; Li, X.; Knox, J. E.; Hratchian, H. P.; Cross, J. B.; Bakken, V.; Adamo, C.; Jaramillo, J.; Gomperts, R.; Stratmann, R. E.; Yazyev, O.; Austin, A. J.; Cammi, R.; Pomelli, C.; Ochterski, J. W.; Ayala, P. Y.; Morokuma, K. ; Voth, G. A.; Salvador, P.; Dannenberg, J. J.; Zakrzewski, V. G.; Dapprich, S.; Daniels, A. D.; Strain, M. C.; Farkas,O.; Malick, D. K.; Rabuck, A. D.; Raghavachari, K; Foresman, J. B.; Ortiz, J. V.; Cui, Q.; Baboul, A. G.; Clifford, S; Cioslowski, J.; Stefanov, B. B.; Liu, G.; Liashenko, A.; Piskorz, P.; Komaromi, I.; Martin, R. L.; Fox, D. J.; Keith, T.; Al-Laham, M. A.; Peng, C. Y.; Nanayakkara, A.; Challacombe, M.; Gill, P. MW.; Johnson, B.; Chen, W.; Wong, M. W.; Gonzalez, C.; Pople, J. A. *Gaussian 03*, revision D.02; Gaussian, Inc.: Wallingford, CT, 2004.

(82) Dunlap, B. I. *J. Chem. Phys.* **1983**, *78*, 3140.

(83) Dunlap, B. I. *J. Mol. Struct (THEOCHEM)* **2000**, *529*, 37.

(84) Byaska, E. J.; de Jong, W. A.; Kowalski, K.; Straatsma, T. P.; Valiev, M.; Wang, D.; Aprà, E.; Windus, T. L.; Hirata, S.; Hackler, M. T.; Zhao, Y.; Fan, P.-D.; Harrison, R. J.; Dupuis, M.; Smith, D. M. A.; Nieplocha, J.; Tipparaju,V.; Krishnan, M.; Auer, A. A.; Nooijen, M.; Brown, E.; Cisneros, G.; Fann, G. I.; Früchtl, H.; Garza, J.; Hirao, K.; Kendall, R.; Nichols, J. A.; Tsemekhman, K.; Wolinski, K.; Anchell, J. ; Bernholdt, D.; Borowski, P.; Clark, T.; Clerc, D.; Dachsel, H.; Deegan, M.; Dyall, K.; Elwood, D.; Glendening, E.; Gutowski, M.; Hess, A.; Jaffe, J.; Johnson, B.; Ju, J.; Kobayashi, R.; Kutteh, R.; Lin, Z.; Littlefield, R.; Long, X.; Meng, B.; Nakajima, T.; Niu, S.; Pollack, L.; Rosing, M.; Sandrone, G.; Stave, M.; Taylor, H.; Thomas, G.; van Lenthe, J.; Wong, A.; Zhang, Z. *NWChem, A Computational Chemistry Package for Parallel Computers, Version 5.0*; Pacific Northwest National Laboratory: Richland, WA 99352-0999, 2006.

(85) Kendall, R. A.; Aprà, E.; Bernholdt, D. E.; Bylaska, E. J.; Dupuis, M.; Fann, G. I.; Harrison, R. J.; Ju, J.; Nichols, J. A.; Nieplocha, J.; Straatsma, T. P.; Windus, T. L.; Wong, A. T. *Comput. Phys. Commun.* **2000**, *128*, 260.

(86) Werner, H.-J.; Knowles, P. J.; Lindh, R.; Manby, F. R.; Schütz, M.; Celani, P.; Korona, T.; Rauhut, G.; Amos, R. D.; Bernhardsson, A.; Berning, A.; Cooper, D. L.; Deegan, M. J. O.; Dobbyn, A. J.; Eckert, F.; Hampel C.; Hetzer, G.; Lloyd, A. W.; McNicholas, S. J.; Meyer W.; Mura, M. E.; Nicklass, A.; Palmieri, P.; Pitzer, R.; Schumann, U.; Stoll, H.; Stone, A. J.; Tarroni, R.; Thorsteinsson, T. MOLPRO, version 2006. 1, a package of ab initio programs. See http://www.molpro.net.

(87) Deegan, M. J. O.; Knowles, P. J. *Chem. Phys. Lett.* **1994**, *227*, 321.

(88) Knowles, P. J.; Hampel, C.; Werner, H.-J. *J. Chem. Phys.* **1993**, *99*, 5219.

(89) Rittby, M.; Bartlett, R. J. *J. Phys. Chem.* **1988**, *92*, 3033.

(90) Li, S. Ph.D. Thesis, University of Kentucky, August, 2004.

(91) Doktorov, E. V.; Malkin, I. A.; Man'ko, V. I. *J. Mol. Spectrosc.* **1977**, *64*, 302.

(92) Yang, D.-S.; Zgierski, M. Z.; Rayner, D. M.; Hackett, P. A.; Mrtinex, A.; Salahub, D. R.; Roy, P. N.; Carrington, T., Jr *J. Chem. Phys.* **1995**, *103*, 5335.

(93) Ruhoff, P. T.; Ratner, M. A. *Int. J. Quantum Chem.* **2000**, *77*, 383.

(94) Gruner, D.; Brumer, P. *Chem. Phys. Lett.* **1987**, *138*, 310.

(95) Kemper, M. J. H.; van Dijk, J. M. F.; Buck, H. M. *Chem. Phys. Lett.* **1978**, *53*, 121.

(96) Li, S.; Dixon, D. A. *J. Phys. Chem. A* **2006**, *110*, 6231.

(97) Moore, C. E. *"Atomic energy levels as derived from the analysis of optical spectra, Volume 1, H to V*; U.S. National Bureau of Standards Circular 467; U.S. Department of Commerce, National Technical Information Service, COM-72-50282: Washington, DC, 1949. The spin-orbit corrections for the atoms are calculated as $\{\sum_J(2J+1)\cdot E_J\}/\{\sum_J(2J+1)\}$.

(98) Chase, M.W., Jr. NIST-JANAF Thermochemical Tables, 4th ed. *J. Phys. Chem. Ref. Data* **1998**, Mono. 9, Suppl. 1.

(99) Cox, J. D.; Wagman, D. D.; Medvedev, V. A. *CODATA Key Values for Thermodynamics*; Hemisphere Publishing Corp.: New York, 1989. The heat of formation for Ti is given in this reference at 298 K. The heat of formation of Ti at 0 K is obtained from this value with the correction from 0 to 298 K given in ref 98.

(100) Curtiss, L. A.; Raghavachari, K.; Redfern, P. C.; Pople, J. A. *J. Chem. Phys.* **1997**, *106*, 1063.

(101) Sherrill, C. D.; Lee, M. S.; Head-Gordon, M. *Chem. Phys. Lett.* **1999**, *302*, 425.

(102) Cohen, R. D.; Sherrill, C. D. *J. Chem. Phys.* **2001**, *114*, 8257.

(103) Li, S.; Dixon, D. A. *J. Phys. Chem. A* **2007**, *111*, 11093.

(104) Huber, K. P.; Herzberg, G. *Molecular Spectra and Molecular Structure IV: Constants of Diatomic Molecules*; Van Nostrand Reinhold: New York, 1979.

(105) Kavan, L.; Grätzel, M.; Gilbert, S. E.; Klemenz, C.; Scheel, H. J. *J. Am. Chem. Soc.* **1996**, *118*, 6716.

JP800170Q